Nonlinear topological photonics ⓕ

ⓘD Daria Smirnova, ⓘD Daniel Leykam, Yidong Chong, et al.

COLLECTIONS

ⓕ This paper was selected as Featured

View Online   Export Citation   CrossMark

ARTICLES YOU MAY BE INTERESTED IN

A semiconductor topological photonic ring resonator
Applied Physics Letters **116**, 061102 (2020); https://doi.org/10.1063/1.5131846

Perspective: Photonic flatbands
APL Photonics **3**, 070901 (2018); https://doi.org/10.1063/1.5034365

Photonic tensor cores for machine learning
Applied Physics Reviews **7**, 031404 (2020); https://doi.org/10.1063/5.0001942

Nonlinear topological photonics ⓕ

View Online   Export Citation   CrossMark

Daria Smirnova,[1] 🆔 Daniel Leykam,[2,3] 🆔 Yidong Chong,[4] and Yuri Kivshar[1,a)] 🆔

AFFILIATIONS

[1]Nonlinear Physics Centre, Research School of Physics, Australian National University, Canberra ACT 2601, Australia

[2]Center for Theoretical Physics of Complex Systems, Institute for Basic Science, Daejeon 34126, Korea

[3]Basic Science Program, Korea University of Science and Technology, Daejeon 34113, Korea

[4]Division of Physics and Applied Physics, School of Physical and Mathematical Sciences, Nanyang Technological University, Singapore 637371

[a)]Author to whom correspondence should be addressed: yuri.kivshar@anu.edu.au

ABSTRACT

Rapidly growing demands for fast information processing have launched a race for creating compact and highly efficient optical devices that can reliably transmit signals without losses. Recently discovered topological phases of light provide novel opportunities for photonic devices robust against scattering losses and disorder. Combining these topological photonic structures with nonlinear effects will unlock advanced functionalities such as magnet-free nonreciprocity and active tunability. Here, we introduce the emerging field of *nonlinear topological photonics* and highlight the recent developments in bridging the physics of topological phases with nonlinear optics. This includes the design of novel photonic platforms which combine topological phases of light with appreciable nonlinear response, self-interaction effects leading to edge solitons in topological photonic lattices, frequency conversion, active photonic structures exhibiting lasing from topologically protected modes, and many-body quantum topological phases of light. We also chart future research directions discussing device applications such as mode stabilization in lasers, parametric amplifiers protected against feedback, and ultrafast optical switches employing topological waveguides.

TABLE OF CONTENTS

I. INTRODUCTION

Topological insulators represent a recently discovered class of solids, which are insulating in their bulk but exhibit special scattering-resistant conducting states on their surfaces, known as topological edge states.[1] The underlying concepts behind these topological edge states are not limited to electronic condensed matter systems, and topological phases can be realized with other physical platforms, including electromagnetic systems such as photonic crystals and metamaterials.[2–4] Currently, we observe rapidly growing interest in the study of topological effects in photonics, motivated by a grand vision of using topological edge states to guide and route light in a manner that is robust against scattering by disorder.

Initial studies of topological effects in photonics were largely inspired by direct analogies with similar effects previously discovered for condensed matter systems, arising from the presence of topologically nontrivial energy bands of electronic band structures. The spectra of electromagnetic waves in periodic media form similar band structures, which can likewise contain topologically nontrivial bands. However, there are a number of important distinctions between photonic systems and their condensed matter counterparts, such as the bosonic nature of photons and the presence of absorption and radiation losses that make photonic systems intrinsically non-Hermitian.[5] Thus, photonics also provides a platform for studying new kinds of topological effects, which have no counterpart in condensed matter. Topological edge states have now been predicted and realized in a wide variety of photonic systems, including gyromagnetic photonic crystals, arrays of coupled optical resonators, metamaterials, helical waveguide arrays, and microcavity polaritons, recently reviewed in Refs. 2–4.

The nonlinear regime is natural to consider at higher optical powers, and therefore, the fundamental question arises: *What effects do nonlinearities have on topological phases and edge states, and vice versa?* In particular, the concept of band topology is inherently tied to linear systems—specifically, the existence of a bandgap structure—and the generalization to nonlinear systems is not straightforward. Nonlinear response in photonics and related fields such as Bose–Einstein condensates is expected to open a door toward advanced functionalities of topological photonic structures, including active tunability, genuine nonreciprocity, frequency conversion, and entangled photon generation[6–14] (see Fig. 1). In addition, nonlinearities may provide a simple way to reconfigure and
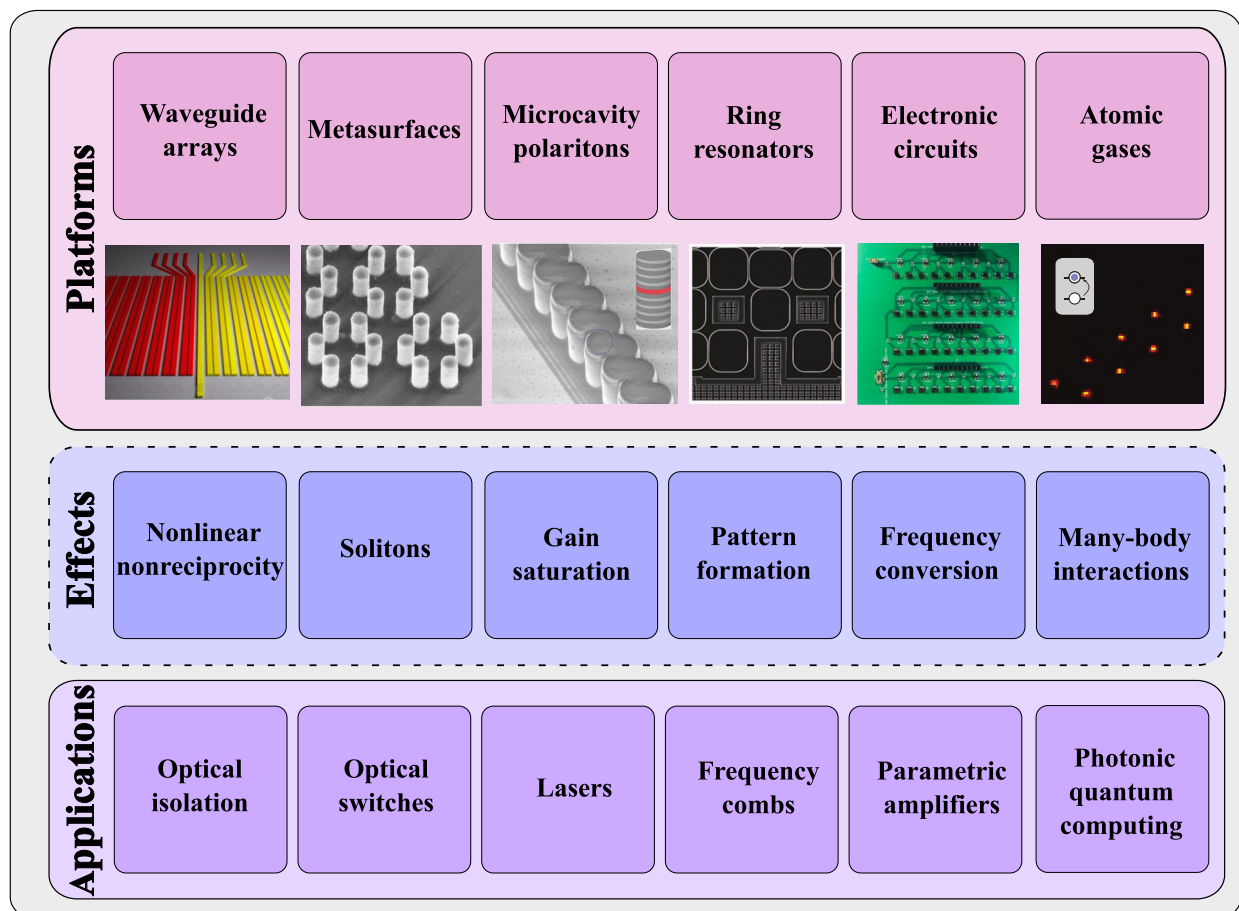

FIG. 1. Basic platforms (top row), selected physical effects (middle row), and potential device applications (bottom row) of nonlinear topological photonics. The fundamental physics of topological phases is combined with nonlinear effects to create advanced functionalities.

control topological waveguides;[15,16] in particular, they are required for ultrafast optical modulation.[17,18] Such studies are still in their initial stages, and they are expected to uncover many surprises.

Here, we review recent advances in the emerging field of nonlinear topological photonics, focusing on the intersection between the studies of topological phases and nonlinear optics. We also describe the broader context of nonlinear effects in other engineered topological systems, including electronic and mechanical metamaterials. However, we omit discussions of Maxwell surface waves[19–22] and the active research topic of using topological electronic materials for nonlinear optics applications.[23–25] Our primary focus here is on artificial topological meta-structures that can be created using mature fabrication techniques and available platforms (silicon, lithography, etc.), which are most feasible for near-term device applications.

This review paper is organized as follows: Sec. II begins with a brief introduction into the field of topological photonics; for detailed reviews, we suggest more comprehensive articles;[2–4] Ref. 3 also includes a brief overview of nonlinear topological photonics up to mid-2018. Section III describes representative topological photonic models that can be employed for the study of nonlinear effects. In Sec. IV, we discuss how to introduce nonlinear effects to topological photonic media. Section V reviews recent theoretical and experimental results on nonlinear localization in topological systems. Nonlinear saturable gain leading to topological lasers is the subject of Sec. VI, followed by the study of topological frequency conversion in Sec. VII. Section VIII discusses the efforts toward realizing topological many-body quantum states of light. Finally, Sec. IX concludes with a discussion of future prospects and open problems.

II. BACKGROUND
A. Topological invariants

Topology is a branch of mathematics concerned with characterizing objects based on their global properties, using *topological invariants*. A topological invariant is a quantity that is unaffected by continuous deformations of the object. For example, a closed 2D surface of any finite 3D object can be characterized by the *genus g*, which counts the number of holes in the object. Thus, a sphere has a genus of $g = 0$, and a torus has a genus of $g = 1$; these two objects cannot transform continuously into each other: Any transformation from a sphere to a torus necessarily involves some discontinuity at which a hole is created; such *topological phase transitions* are accompanied by a stepwise (quantized) change in a topological invariant.

Crucially, global topological properties such as the genus can be related to local geometrical properties via the Gauss–Bonnet theorem, which states that topological invariants can be calculated by integrating some local field strength over the entire surface. For example, the genus can be computed by integrating the local Gaussian curvature over the entire surface.

Under certain conditions, topological invariants can be used to describe band structures of periodic crystalline materials. In this context, continuous transformations are those that preserve all symmetries of system and do not close the bandgap, and a topological phase transition requires the bandgap to close and re-open. Boundaries between two materials characterized by distinct topological invariants necessarily host special gapless states localized to the boundary. These states are robust in the sense that they can only be removed by a change in one of the bulk topological invariants. This important relationship between bulk topology and the existence of boundary states is known as the *bulk-boundary correspondence*.

The dimension of the system plays an important role in the classification and properties of topological phases,[26] as shown in Fig. 2. Topological boundary states can occur at the ends of one-dimensional (1D) systems, the edges of a two-dimensional (2D) systems, or the surfaces of a three-dimensional (3D) systems, as shown schematically in Fig. 2 (upper row). Generally, an N dimensional topological insulator has N dimensional gaped bulk states and $(N-1)$ dimensional boundary states. For example, the boundaries of 1D systems are end points, and 1D topological insulators host end states whose energies are pinned to the middle of the bandgap. Note that while the dimension N is usually assumed to be the physical dimension of the system, one can also employ internal degrees of freedom, such as orbital angular momentum, as additional synthetic dimensions to realize higher-dimensional topological phases.[27,28]

B. Topological insulators

The 2D case has been particularly important for the development of the field. The first known example of a topological insulator phase was the *quantum Hall* (QH) phase discovered in 1980, which emerges in 2D systems with broken time-reversal (TR) symmetry, e.g., in the presence of a strong magnetic field.[29] The corresponding bulk topological invariant is the Chern number C.[30] The topological boundary states of the QH phase are called chiral edge states and propagate unidirectionally along the boundary, immune to backscattering from disorder. In 2005, a generalization to insulators preserving time-reversal symmetry and exhibiting strong spin–orbit interactions was discovered by Kane and Mele, known as the *quantum spin-Hall* (QSH) phase.[31] In its simplest form, the Kane–Mele model is essentially two copies of the QH phase, where up and down-spin electrons are decoupled and experience opposite effective magnetic fields. Although

(N-1)D topological states
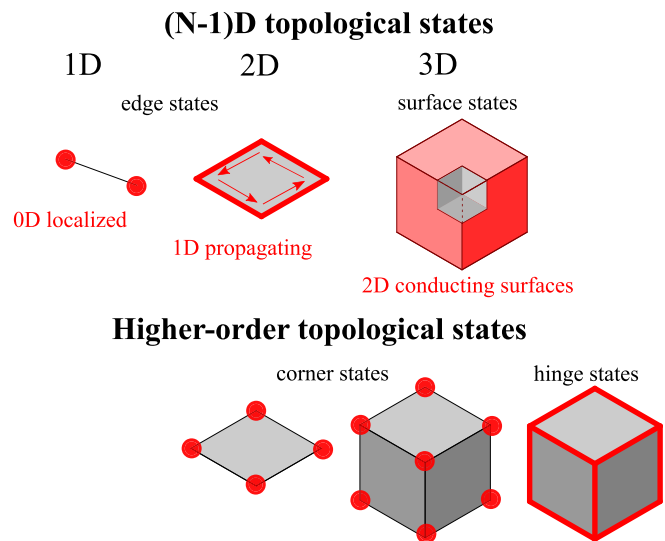
Higher-order topological states

FIG. 2. Topological classes in different dimensions. Conventional topological insulators are insulating in a bulk but conducting via gapless states at their edges or surfaces. Higher-order topological insulators have topological states at corners or hinges.

the net Chern number is zero due to TR symmetry, one can formulate a spin Chern number $C^{\text{spin}} = (C_\downarrow - C_\uparrow)/2$, which is nonzero in the QSH phase. The QSH phase supports pairs of counter-propagating edge modes with opposite spins, called helical edge states, which are protected from backscattering into each other as long as time-reversal is preserved. Interestingly, this protection can hold even in the presence of spin-mixing interactions that make C^{spin} ill-defined; this more general case is described by a binary Z_2 invariant.[1] Subsequently, the QSH phase was observed in quantum well hetero-structures,[32,33] whose spectrum of edge states was in fact first calculated back in the 1980s.[34,35]

The discovery of the QSH phase and Z_2 invariant sparked broad interest in topological insulators, and a large "zoo" of topological materials with various symmetries and dimensions have since been discovered.[36] Particularly important for photonics applications are topological crystalline insulators (TCI) and valley-Hall (VH) insulators: these are similar to the QSH phase in that they exhibit protected counter-propagating edge states, however, they replace the electron spin with pseudospin degrees of freedom associated with point-group symmetries such as rotation[37] and inversion.[38,39]

Topological phases also exist in periodically modulated systems, which can be characterized by the Floquet band structures describing states that remain invariant (up to a phase factor) when viewed at integer multiples of the driving period. When the driving frequency is large, the Floquet band structure can be understood in terms of static effective Floquet Hamiltonians.[40,41] On the other hand, low-frequency driving gives rise to topological phases unique to driven systems[42] and allows topological adiabatic pumping between edge modes via bulk modes.[43]

Recently, new classes of the so-called *higher-order* topological insulators in dimensions $N > 1$ have been discovered.[44] Higher-order topological insulators have $(N-1)$-dimensional boundaries that, unlike those of conventional topological insulators, do not exhibit gapless states but instead constitute topological insulators themselves. An n-th order insulator has gapless states on an $(N-n)$-dimensional subsystem. For instance, in three dimensions, a second-order topological insulator has gapless states on the 1D hinges between distinct surfaces, and a third-order topological insulator has gapless states on its 0D corners, as shown in Fig. 2 (lower row). Similarly, a second-order topological insulator in 2D also has mid-gap corner states.

C. Photonic topological insulators

There are numerous approaches to engineering photonic analogs of topological insulators,[2,4,45–48] which can be subdivided into TR-broken systems, which require an external magnetic bias or time modulation, and TR-preserved routes, which do not. Some notable 2D topological photonic phases and systems are illustrated in Figs. 3 and 4, following Ref. 46. In many cases, the structures are designed to emulate topological materials studied in condensed matter physics.[49]

Photonic analogs of QH systems can be realized via gyroelectric or gyromagnetic photonic crystals, where the gyrotropy effect breaks TR symmetry. The first demonstration of backscattering-immune photonic topological edge states with the use of a gyrotropic microwave photonic crystal was performed by Wang *et al.* in 2009,[50] following a theoretical proposal by Raghu and Haldane.[54–56] However, this approach is challenging to scale to optics due to the difficulty in integrating magnetic materials with optical circuity, and the fact that magnetic responses are weak at optical frequencies. Thus, TR-preserving

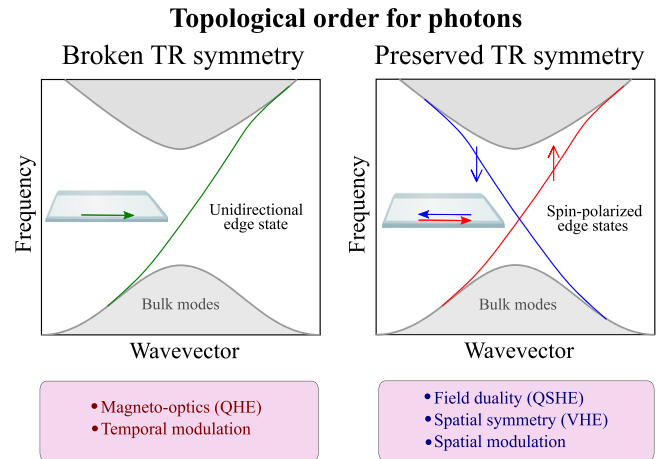### Topological order for photons

FIG. 3. Schematic of the spectra for two distinct types of topologically nontrivial photonic systems in 2D with broken (left column) and preserved (right column) TR symmetry. The structures are designed to emulate the quantum Hall effect (QHE) and quantum spin- and valley-Hall effects (QSHE and VHE). Gray shaded regions in band diagrams depict the continuum of the extended bulk states with insulating gaps. The bulk bandgaps are traversed by gapless edge states (colored dispersion lines). These edge states are topologically protected from backscattering and propagate along the interfaces of topologically inequivalent materials as illustrated in insets. The TR-invariant system supports a pair of counter-propagating edge states with their spin locked to their momentum (spin-momentum locking). Spin-up and spin-down states are shown with red and blue arrows, respectively.

approaches have been more widely pursued, as they are compatible with a large variety of platforms including waveguide arrays,[51,57] coupled resonators,[58] photonic crystals,[53] and metamaterials.[59]

For example, Rechtsman *et al.* implemented a waveguide array that acts as a Floquet photonic topological insulator in the optical frequency domain.[51] The waveguides are twisted so that inter-waveguide tunneling is accompanied by phase accumulation, similar to a gauge field; hence, the propagation of light in the array is similar to the time evolution of 2D electrons in a magnetic field. Notably, the waveguide array itself preserves TR symmetry; the sign of the effective magnetic field depends on the direction of propagation along the waveguide array axis.

Another breakthrough approach used arrays of coupled optical ring resonators[58,60] in the near-infrared ($1.55\,\mu$m). Here, each ring supports degenerate clockwise and counterclockwise modes, forming a spin degree of freedom. A spin-dependent gauge field is implemented by auxiliary coupling rings with different optical path lengths. The overall structure obeys TR symmetry, with the sign of the effective magnetic field depending on whether the clockwise or counterclockwise mode is considered, forming a QSH phase.

Other photonic QSH systems have also been implemented, including bianisotropic photonic crystals, with the magnetoelectric coupling serving in the role of spin–orbit interaction,[61–63] as well as TCIs and VH phases based on nonmagnetic photonic crystal slabs,[16,37,64–70] electronic circuits,[71,72] and metacrystals containing overlapping electric and magnetic dipolar resonances specially designed to satisfy electromagnetic duality.[52,59]

We emphasize a common feature of all the structures listed above. The standard electromagnetic TR symmetry alone is

Topological photonic structures

Bianisotropic metacrystals
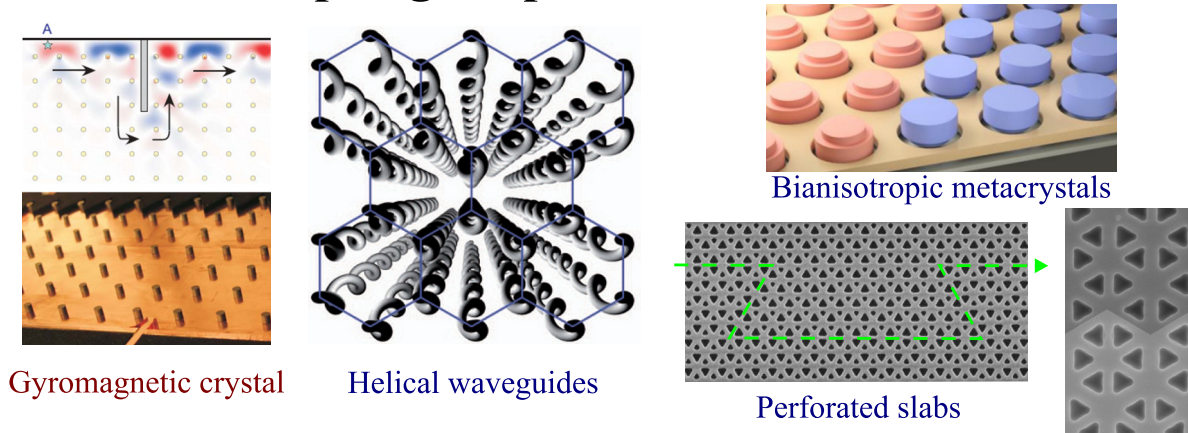
Gyromagnetic crystal   Helical waveguides

Perforated slabs
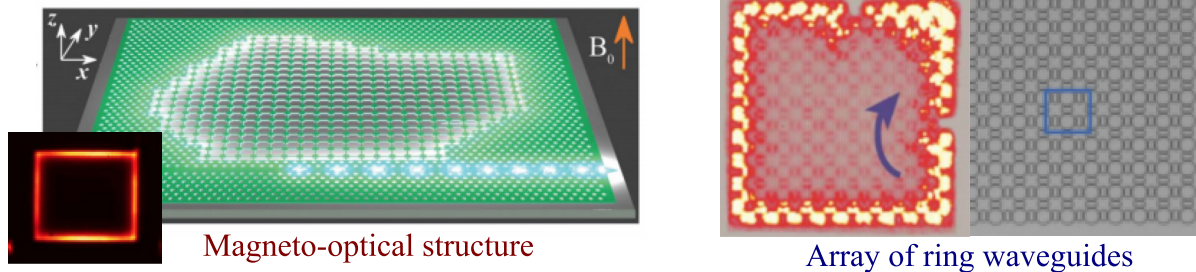
Topological lasing cavities

Magneto-optical structure   Array of ring waveguides

FIG. 4. The TR-broken and TR-preserved designs from Fig. 3 are illustrated by images of the photonic structures fabricated for specific applications in microwaves and optics,[8,16,50–53] one of which is topological lasers. These include magnetically biased photonic crystals, waveguide arrays, ring resonator lattices, metacrystals of bianisotropic disks, and nanopatterned dielectric slabs. Images adapted with permissions from Rechtsman *et al.*, Nature **496**, 196 (2013). Copyright 2013 Nature Springer; Shalaev *et al.*, Nat. Nanotechnol. **14**, 31 (2018). Copyright 2018 Nature Springer; Bahari *et al.*, Science **358**, 636–640 (2017). Copyright 2017 The American Association for the Advancement of Science; Bandres *et al.*, Science **359**, eaar4005 (2018). Copyright 2018 The American Association for the Advancement of Science.

insufficient to protect the QSH phase, and other internal symmetries such as duality[61] or point group symmetries[37] are required; the edge state robustness is conditional on these internal symmetries also being preserved. Imperfections in real samples can therefore cause the topological properties to break down, so photonic topological edge states are only protected from scattering on defects of certain types and are overall less robust than topological edge states in condensed matter systems.

III. TOPOLOGICAL LATTICE MODELS

The key features of topological bands, including their interface states, can be understood by studying simple discrete lattice models. This section introduces some basic lattice designs known to exhibit topological transitions in the linear regime. They can be formulated in terms of abstract tight binding models for 1D and 2D arrays, illustrated in Fig. 5.

A. Basic concepts

According to Bloch's theorem, the spectrum of any periodic lattice forms a band structure, where energy eigenvalues $\mathscr{E}_n(\mathbf{k})$ form a

discrete set of bands indexed by n, and the Bloch momentum $\mathbf{k}$ is restricted to the lattice's Brillouin zone. The corresponding eigenstates are Bloch waves $\psi_n = \mathbf{u}_n(\mathbf{k}, \mathbf{r})e^{i\mathbf{k}\mathbf{r}}$, where the Bloch function $\mathbf{u}_n(\mathbf{k}, \mathbf{r})$ shares the same spatial $\mathbf{r}$ periodicity as the lattice, and is, in general, a vector encoding internal degrees of freedom such as the spin or polarization of the field. Topological properties of lattices are dictated by the behavior of the Bloch functions as $\mathbf{k}$ is varied.

One fundamental property of the Bloch waves is their Berry phase,[73] which can be calculated as a line integral along a closed path in $\mathbf{k}$ space as $\gamma_n = \oint \mathbf{A}_n \cdot d\mathbf{k}$, where $\mathbf{A}_n(\mathbf{k}) = \langle \mathbf{u}_n | i\nabla_{\mathbf{k}} | \mathbf{u}_n \rangle$ is the Berry connection. Here, the inner product defined by the bra-ket notation is spatial integration over a single unit cell. Roughly speaking, the Berry connection provides a measure of how the form of the Bloch function (e.g., its polarization) changes along the given path. Using Stokes' theorem, the Berry phase can be alternatively computed as an integral over the area enclosed by the path: $\gamma_n = \int\int \mathbf{F}_n d^2\mathbf{k}$, where $\mathbf{F}_n = \nabla_{\mathbf{k}} \times \mathbf{A}_n$ is the Berry curvature.

The Berry connection and curvature are strongly reminiscent of the vector potential and magnetic field in the theory of electromagnetism. For example, the Berry connection is gauge-dependent:
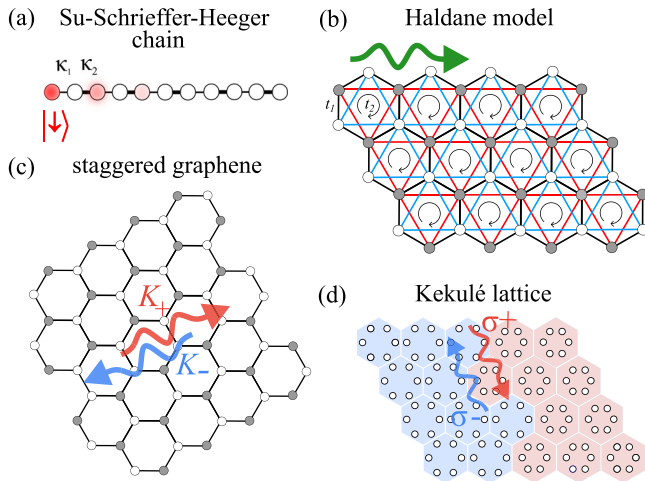
FIG. 5. Schematics of topological lattices. (a) SSH array of dimers (1D chiral chain) created by alternating coupling strengths $\kappa_1 < \kappa_2$ between nearest-neighbor elements. In a finite chain terminated at the weak bond, the edge-bound state shown in reddish color represents a staggered mode localized at one sublattice (pseudo-spin down) with the decay factor defined by the coupling imbalance. (b) Haldane model on a honeycomb lattice with complex next-nearest-neighbor hopping that breaks TR symmetry and creates pseudo-magnetic flux (QHE). The green wavy arrow illustrates a chiral edge state. (c) Staggered graphene composed of two interpenetrating triangular sublattices (shown as open and filled circles) with different on-site potentials. The domain wall created by inversion of a staggered sublattice potential guides chiral valley-polarized ($K_{\pm}$) edge states shown with red and blue wavy arrows (VHE). (d) Hexagonal Kekulé lattice of expanded/shrunken hexamers. The interface between two domains supports a pair of topologically protected, spin-momentum locked edge states with opposite helicities $\sigma^{\pm}$ (QSHE).

transforming the Bloch functions as $\mathbf{u}_n(\mathbf{k}) \rightarrow \mathbf{u}_n(\mathbf{k})e^{i\varphi(\mathbf{k})}$ modifies the Berry connection as $\mathbf{A}_n \rightarrow \mathbf{A}_n - \nabla_{\mathbf{k}}\varphi(\mathbf{k})$. On the other hand, the Berry phase and Berry curvature are gauge-invariant quantities that can be related to physical observables. Integrating the Berry curvature over a 2D Brillouin zone yields the quantized Chern number C_n, which characterizes QH topological phases. The Chern number counts the winding (the number of complete turns) of the phase evolution of the eigenvector upon encircling the entire Brillouin zone.

Often one is only interested in the dynamics within a narrow range of energies, such that only a few bands are relevant. In this case, the dynamics can often be captured by effective discrete lattice Hamiltonians, written in second quantized notation as

$$\hat{H} = \sum_{i,j} H_{ij}\hat{a}_i^{\dagger}\hat{a}_j, \tag{1}$$

where $\hat{a}_i^{\dagger}$ ($\hat{a}_i$) creates (annihilates) an excitation at the ith site, off diagonal matrix elements H_{ij} describe couplings between sites i and j (e.g., due to evanescent coupling), and the diagonal elements H_{ii} describe site energies (e.g., determined by the local refractive index).

Owing to the translation invariance of the lattice, performing a Fourier transform block diagonalizes $\hat{H}$ to a Bloch Hamiltonian $\hat{H}(\mathbf{k})$. If there are m degrees of freedom per unit cell, $\hat{H}(\mathbf{k})$ is an $m \times m$ Hermitian matrix, which results in an m band lattice model. Each eigenvalue of $\hat{H}(\mathbf{k})$ gives the dispersion relation of one of the bands of interest, with corresponding eigenvectors defining the Bloch functions $\mathbf{u}_n(\mathbf{k})$, which are now m-component vectors.

In all one-band models, the Bloch functions are trivial; as one component vectors, there is no way for their direction to vary with $\mathbf{k}$, and therefore, the Berry connection and curvature necessarily vanish. Thus, the simplest models of topological phases involve two bands.

The most general two band Hermitian Bloch Hamiltonian can be written as $\hat{H}(\mathbf{k}) = \mathbf{h}(\mathbf{k}) \cdot \hat{\boldsymbol{\sigma}}$ and has eigenvalues $\mathscr{E}_{\pm}(\mathbf{k}) = \pm|\mathbf{h}(\mathbf{k})|$, where $\hat{\boldsymbol{\sigma}} = (\hat{\sigma}_x, \hat{\sigma}_y, \hat{\sigma}_z)$ is a vector of the three Pauli matrices. In many cases, the topological properties of the lattice model can be captured in the continuum limit by Taylor expanding $\mathbf{h}(\mathbf{k})$ for small displacements $\delta\mathbf{k}$ about some point of interest in the Brillouin zone to obtain a Dirac-like Hamiltonian, which, e.g., in 2D systems, take the form

$$\hat{H}_D(\delta\mathbf{k}) = v_D(\delta k_x\hat{\sigma}_x + \delta k_y\hat{\sigma}_y) + m\hat{\sigma}_z, \tag{2}$$

where v_D is a velocity parameter and m is an effective mass, which determines the size of the bandgap.

When $m = 0$, Eq. (2) describes a conical intersection with linear dispersion relation $\mathscr{E}_{\pm} = \pm v_D|\delta\mathbf{k}|$ resembling that of massless fermions.[74] These continuum models can be generalized to a larger number of bands. For example, certain three band intersections are described by the effective continuum Hamiltonian

$$\hat{H}_M(\delta\mathbf{k}) = v_D(\delta k_x\hat{S}_x + \delta k_y\hat{S}_y), \tag{3}$$

expressed through spin-1 matrices; its three eigenvalues are $\mathscr{E}_0 = 0$, $\mathscr{E}_{\pm} = \pm v_D|\delta\mathbf{k}|$, corresponding to a zero energy flatband and two linearly dispersing modes.

B. Su–Schrieffer–Heeger model

The simplest lattice that exhibits topological modes is the Su–Schrieffer–Heeger (SSH) model, which describes a 1D dimer chain with alternating weak and strong nearest-neighbor couplings $\kappa_{1,2}$ [see Fig. 5(a)]. In the second quantized notation, the many-body Hamiltonian is

$$\hat{H}_{SSH} = -\sum_{j=1}^{N}\left(\kappa_1\hat{a}_j^{\dagger}\hat{b}_j + \kappa_2\hat{a}_{j+1}^{\dagger}\hat{b}_j + h.c.\right), \tag{4}$$

where $\hat{a}_j^{\dagger}$, $\hat{b}_j^{\dagger}$ ($\hat{a}_j$, $\hat{b}_j$) denote creation (annihilation) operators at A or B sublattices of the jth unit cell. By Fourier transformation, Eq. (4) returns the single-particle Bloch Hamiltonian in the momentum representation

$$\hat{H}_{SSH}(k) = -[\kappa_1 + \kappa_2\cos(kd)]\hat{\sigma}_x - \kappa_2\sin(kd)\hat{\sigma}_y, \tag{5}$$

where d is a lattice spacing. The two bands $\mathscr{E}_{\pm}$ are separated by a gap when $\kappa_1 \neq \kappa_2$, with the closure of the bandgap when $\kappa_1 = \kappa_2$ forming a transition between two distinct topological phases, described by the 1D Berry phase, also known as the Zak phase,[75] which takes the quantized values π (in the nontrivial case, $\kappa_2 > \kappa_1$) or 0 (in the trivial case, $\kappa_2 < \kappa_1$).

In finite lattices whose terminations break the stronger coupling ($\kappa_2 > \kappa_1$), there exist edge states in the middle of the bandgap. These states are localized in one sublattice and decay exponentially away from the lattice edge, at a rate determined by the size of the gap. These states are protected in the sense that their frequency is pinned to zero and they cannot be destroyed by any perturbation that respects the chiral symmetry $\hat{\sigma}_z\hat{H}_{SSH}(k)\hat{\sigma}_z = -\hat{H}_{SSH}(k)$, as long as the two bands remain separated by a gap.

More generally, one can introduce the winding number $\nu = \frac{1}{2\pi} \oint d\arg[h(k)]$, where $h(k) = h_x(k) + i h_y(k)$, which counts the number of times the curve traced out by the vector $\mathbf{h}(k) = -[\kappa_1 + \kappa_2 \cos kd, \kappa_2 \sin kd, 0]$ encloses the origin of the (h_x, h_y) plane. The winding number is equal to the number of edge states for Hamiltonians with chiral symmetry. For example, in the SSH model $\nu(\kappa_2 > \kappa_1) = 1$ or $\nu(\kappa_2 < \kappa_1) = 0$, indicating a topological transition at $\kappa_2 = \kappa_1$.

C. Honeycomb lattices

The prototypical model for studying 2D topological phases is the honeycomb lattice, which can be used to implement optical analogs of graphene (i.e., *photonic graphene*).[51,54,55,76–83] This lattice has a hexagonal Brillouin zone, whose inequivalent corners (called the $K_\pm$ points) host conical intersection degeneracies protected by TR and parity P (spatial inversion) symmetries. Breaking either symmetry lifts the degeneracies and opens a bandgap. Breaking P creates a trivial gap, because the Berry curvatures at the $K_\pm$ points have opposite signs, yielding a vanishing Chern number. Breaking TR symmetry generates a nontrivial topological phase, with the Berry curvature having the same sign at the $K_\pm$ points.

These features are captured by the Haldane model,[84] which exhibits tunable transitions between trivial and topological phases. In particular, TR is broken using complex-valued next-nearest-neighbor (NNN) couplings, see a schematic in Fig. 5(b). To ensure that the Brillouin zone is unaltered by the TR symmetry breaking, the couplings are staggered so that there is no net magnetic flux per unit cell: encircling one lattice plaquette clockwise (counterclockwise) gives a phase factor of $e^{i\phi}$ ($e^{-i\phi}$). The lattice Hamiltonian is

$$\hat{H}_{\text{Haldane}} = m_I \sum_{\langle i \rangle} \left(\hat{a}_i^\dagger a_i - \hat{b}_i^\dagger b_i \right) - t_1 \sum_{\langle i,j \rangle} \left(\hat{a}_i^\dagger \hat{b}_j + \hat{b}_j^\dagger \hat{a}_i \right)$$
$$- t_2 \left[e^{i\phi} \sum_{\langle\langle i,j \rangle\rangle} \hat{a}_i^\dagger \hat{a}_j + e^{-i\phi} \sum_{\langle\langle i,j \rangle\rangle} \hat{b}_i^\dagger \hat{b}_j + h.c. \right], \quad (6)$$

where $\langle i,j \rangle$ and $\langle\langle i,j \rangle\rangle$ denote summations over the first and second nearest neighbors sites, respectively, t_1 and t_2 are the hopping amplitudes, and m_I is a parameter that breaks inversion symmetry via sublattice detuning. Near the $K_\pm$ points, the effective continuum Hamiltonian is

$$\hat{H}_{K_\pm}(\delta\boldsymbol{k}) = 3t_2 \cos\phi + v_D \left(\pm \delta k_x \hat{\sigma}_x + \delta k_y \hat{\sigma}_y \right)$$
$$+ \left(m_I \pm 3\sqrt{3} t_2 \sin\phi \right) \hat{\sigma}_z, \quad (7)$$

where $v_D = \sqrt{3} t_1/2$. Thus, the effective mass due to TR breaking has opposite signs at the two valleys, whereas the effective mass due to P

breaking has the same sign at both valleys. The band structure of Eq. (6) can be characterized by the Chern number, which is non-zero when the gap is dominated by the TR breaking terms; in this regime, chiral edge modes are guaranteed to exist along the boundary of the finite lattice. Systems similar to the Haldane model are known as *Chern insulators*.

A honeycomb lattice with preserved TR symmetry but broken P (space-inversion) symmetry is a VH insulator, see Fig. 5(c). The domain walls separating VH lattices that have opposite P breaking host chiral edge states.[39] For small P breaking, the Berry curvatures are strongly localized at the valleys, and the local integrals around $K_\pm$ valleys take non-zero quantized values of $\pm\pi$ for each band, which yields a valley Chern number $C^{\text{valley}} = \pm 1/2$. Flipping the sign of the P breaking also flips the sign of the Berry curvature in each valley. Across a domain wall, there is a difference of ± 1 between valley Chern numbers, resulting in one family of topological edge states in each valley.

Another honeycomb lattice variant that is extremely useful for topological photonics is a topological crystalline insulator devised by Wu and Hu.[37] It involves clustering neighboring plaquettes of 6 lattice sites by alternately widening or narrowing the inter-site separations [see Fig. 5(d)]. This clustering causes the $K_\pm$ points to be folded onto the center of the Brillouin zone (the Γ point); the interaction of the overlaid Dirac cones causes a bandgap to open. The corresponding effective Hamiltonian is of the Bernevig–Hughes–Zhang QSH Hamiltonian,[32] where the role of spin is played by angular momentum eigenstates of the lattice's C^6 point group symmetry. The model exhibits helical edge states at the boundaries between domains with shrunken (trivial) and expanded (nontrivial) clusters.

The continuum Hamiltonians and topological invariants discussed in this section are listed in Table I.

IV. PLATFORMS FOR NONLINEAR TOPOLOGICAL SYSTEMS

The linear lattice models discussed in Sec. III are agnostic about length and frequency scales and the wave amplitudes involved. Indeed, these models have been implemented at characteristic frequencies ranging from the optical range (10^{14} Hz) to microwaves (10^9 Hz) and electronics (10^6 Hz), using platforms such as arrays of coupled waveguides, microring resonators, and photonic crystals. When studying nonlinear phenomena, however, this universality is lost. This section provides an overview of different platforms for nonlinear topological photonics, summarized in Table II.

Much of the older literature on nonlinear effects in periodic lattices was written before topological effects came into focus, and, therefore, mainly dealt with the consequences of bandgaps and

TABLE I. Continuum Hamiltonians of common 2D topological models employed in photonics. Here, the Pauli matrices $\hat{\sigma}$, $\hat{\tau}$, $\hat{s}$ act on the sublattice, valley and spin degrees of freedom, respectively. m_T, m_I are the mass terms induced by TR and P symmetry reductions; m_{SO} is responsible for the effective spin–orbit interaction.

Model	Hamiltonian	Topological invariant
Haldane	$\hat{H} = v_D(\hat{\sigma}_x \hat{\tau}_z \delta k_x + \hat{\sigma}_y \hat{\tau}_0 \delta k_y) + \hat{\sigma}_z(\hat{\tau}_z m_T - \hat{\tau}_0 m_I)$	Chern number $C = \frac{1}{2}(\text{sgn}(m_I - m_T) - \text{sgn}(m_I + m_T))$
Kane–Mele	$\hat{H} = v_D \hat{s}_0(\hat{\sigma}_x \hat{\tau}_z \delta k_x + \hat{\sigma}_y \hat{\tau}_0 \delta k_y) + \hat{\sigma}_z \hat{\tau}_z \hat{s}_z m_{SO}$	Spin Chern number $C^{\text{spin}} = \text{sgn}(m_{SO})$
Bernevig–Hughes–Zhang	$\hat{H} = v_D(\hat{\sigma}_x \hat{s}_x \delta k_x + \hat{\sigma}_y \hat{s}_0 \delta k_y) + \hat{\sigma}_z \hat{s}_0(m + \beta \delta k^2)$	Spin Chern number $C^{\text{spin}} = \frac{1}{2}(\text{sgn } m - \text{sgn } \beta)$
Staggered graphene	$\hat{H} = v_D(\hat{\sigma}_x \hat{\tau}_z \delta k_x + \hat{\sigma}_y \hat{\tau}_0 \delta k_y) - \hat{\sigma}_z \hat{\tau}_0 m_I$	Valley Chen number $C^{\text{valley}} = \pm \frac{1}{2}\text{sgn}(m_I)$

TABLE II. Examples of different platforms employed for nonlinear topological photonics. Frequency and power scales quoted are the data taken from the specific works cited.

Platform	Material	Spectral range	Power, duration	Source
Optical waveguides	AlGaAs	1530 nm	500 W, 100 fs	87
	Fused silica	800 nm	1 MW, 100 fs	88
	Photorefractives	488 nm	mW, CW	89
	Lithium niobate	1550 nm	4 kW, 9 ps	90
	Chalcogenides	1040 nm	10kW, 300 fs	91
Optical resonators	Si microrings	1550 nm	85 μW, CW	92
	InP PhC slab	1587 nm	200 μW, CW	93
	GaAs/InAs PhC slab	1040 nm	150 μW, 20 ns	94
	Si metasurfaces	1550 nm	200 mW, 300 fs	69
	Fiber loops	1555 nm	120 mW, 50 ns	95
	Exciton–polaritons	780 nm	10 mW, CW	96
Atomic gases	Warm ^{85}Rb vapor	795 nm	1 mW, CW	97
	Ultracold ^{87}Rb gas	780 nm	Single photon, 10 ms	98
Metamaterials	Split ring resonators	1.5 GHz	1 W, CW	99
	Circuit QED	5 GHz	Single photon, 100 ns	100
	RF circuits	100 MHz	300 mW, CW	101

discreteness, while overlooking the role of topology. For instance, many works have studied how nonlinearity affects non-topological surface states, which are typically generated by defects or localized potentials along the boundary of a lattice. For example, a semi-infinite array of coupled quantum wells can form surface states if the energy of the first well is detuned from the energy of the other wells. Such threshold conditions are typical of (topologically trivial) Tamm surface states.[85] In the nonlinear regime, it has been shown that self-trapping can overcome surface repulsion, inducing localized modes near the edge of a discrete lattice above a certain power threshold.[86] On the other hand, topological lattice models support edge states even in the low-amplitude limit and do not require any threshold perturbation to exist.

Since nonlinear problems are generally much harder to solve, platforms where the full set of Maxwell's equations can be well approximated by simpler coupled-mode or tight-binding lattice models are preferred for studying nonlinear topological photonics.

A. Waveguides

Nonlinear effects naturally emerge in waveguide lattices due to the intrinsic nonlinearity of the host medium. For example, the intensity-dependent refractive index of cubic nonlinear materials enters tight binding models as a nonlinear on-site potential. One of the advantages of waveguide lattices is that even though the bulk material nonlinearity can be quite weak, the important parameter governing the dynamics is the ratio of the nonlinearity to the linear coupling coefficient. Therefore, provided one has access to a sufficiently long propagation distance and effects such as absorption remain negligible, one can reduce the coupling to increase the effective nonlinearity and observe effects such as optical switching and spatial solitons.

Nonlinear photonic waveguide lattices have a long history, dating back to the seminal prediction of optical discrete solitons by Christodoulides and Joseph in 1988.[102] The first experiments by

Eisenberg *et al.* in 1998[87] used femtosecond laser pulses in a cubic nonlinear 1D AlGaAs waveguide array. The following decade saw several breakthroughs, including the observation of discrete solitons in photorefractive crystals using continuous wave beams,[89] laser-written waveguide arrays in fused silica glass,[88] and quadratic nonlinear lithium niobate waveguides.[90] For details, see Refs. 103–105.

The main challenge in generalizing these previous experiments to topological waveguide lattices is that there is a trade-off between ease of fabrication and ease of observing nonlinear effects. For example, AlGaAs, lithium niobate, and photorefractive waveguide arrays have strong nonlinearity, but are presently limited to simple 1D topological lattices such as the SSH model. Alternatively, fused silica glass waveguides created using laser writing can readily form 2D topological lattices, but the nonlinearity is much weaker, demanding shorter pulses with higher peak powers and increasing the complexity of experiments and modeling. For example, beam shaping is required to avoid material damage when exciting the waveguides and modeling should take into account effects such as material dispersion and two photon absorption.[106] Moreover, many theoretical proposals are based on models of nonlinear coupling, which is negligible in this platform.

B. Microcavities

Optical cavities, supporting whispering-gallery, Fabry–Pérot, or Mie-type resonances are able to efficiently trap light. Therefore, optical resonator lattices, such as microring arrays and particle metasurfaces, can enhance nonlinear effects and thus significantly lower optical power requirements, but at the expense of operating bandwidth. Additionally, the ability to tailor the pump beam or embed different materials onto the resonators gives access to a variety of nonlinear effects. For example, continuous wave operation leads to strong thermal nonlinearities due to absorption-induced heating of microresonators,[92] while two-photon absorption results in nonlinear resonance shifts due to free carrier dispersion.[93] Unfortunately, the mechanisms

that provide the strongest self-action effects are also intrinsically lossy, although losses can be compensated via integration of gain media such as quantum wells.[94,95]

Most experiments with nonlinear topological resonator lattices have been limited to perturbative regimes, which are easier to analyze and support effects such as lasing (Sec. VI) and harmonic generation (Sec. VII). For self-action effects (e.g., bistability and nonlinear non-reciprocity), it has been preferable to use only a few nonlinear elements to avoid complications such as multistability or instability.[92,93] There are two exceptions where self-action effects are observable in nonlinear propagation dynamics: pulse propagation in coupled fiber loops[95,107] and exciton-polariton condensates in microcavities.[108]

C. Nanophotonic structures

In the last five years, nanostructures made of high-index dielectric materials,[109] with judiciously designed resonant elements and lattice arrangements, have shown special promise for practical implementations of nonlinear topological photonics.[11,15,16,65–67,69] This approach bridges the fundamental physics of topological phases with resonant nanophotonics and multipolar electrodynamics.[110]

The high-index dielectric nanostructures typically employed for topological nanophotonics possess strong optical nonlinearities enhanced by Mie-type resonances. In particular, silicon has a strong bulk third-order optical susceptibility,[111,112] while III–V noncentrosymmetric semiconductors are favorable for efficient second-order nonlinear applications due to a large volume quadratic nonlinearity.[113,114] The resonant near-field enhancement associated with excitation of multipolar Mie modes in high-permittivty dielectric nanostructures further facilitates the nonlinear processes at the nanoscale.

Already a few topological nanostructures that support subwavelength edge states and convert infrared radiation into visible light have been proposed and experimentally verified.[11,69] Due to compactness and robustness to fabrication imperfections, topological nanophotonics is also being pursued for quantum information transport in integrated photonic platforms.[66] We discuss these applications further in Sec. VII.

D. Atomic gases

Optical beams resonant with atomic transitions provide perhaps the strongest optical nonlinearities available for topological photonics, supporting even single photon (quantum) interactions provided the atoms are placed in an optical cavity and cooled to ultra-low temperatures.[98,115,116] Novel quantum many-body states accessible in this regime are discussed further in Sec. VIII.

One can also employ atomic gases in a waveguide configuration, enabling the study of nonlinear propagation dynamics. In this case, a bright beam coupled to a transition of a three level atom controls the effective refractive index seen by a weaker probe beam. Very recent experiments have demonstrated induction of honeycomb lattices using this approach.[82,97] A big advantage compared to non-resonant nonlinearities is that both the sign and magnitude of the Kerr nonlinear response seen by the probe beam can be adjusted just by slightly changing its frequency. Moreover, by pumping an additional atomic energy level, one can also introduce a Raman gain, enabling the study of various non-Hermitian photonic lattices.[117] Thus, atomic gases provide a highly promising platform for both nonlinear and non-Hermitian topological photonics.

E. Microwave metamaterials

In the microwave regime, nonlinearities are much harder to realize than in optics (unlike most other photonic phenomena). One approach is to insert nonlinear electronic lumped elements, like varactor diodes, into microwave metamaterials such as split ring resonators.[99] This can yield mean-field nonlinear effects under a pump power of ≈ 1 W. Alternatively, one can construct photonic crystals out of materials exhibiting nonlinear susceptibilities at microwave frequencies.[118]

Ultra-strong single photon nonlinearities are accessible by coupling microwave cavities to superconducting qubits such as Josephson junctions,[100,119,120] although this introduces the additional experimental complication of cryogenic operating temperatures. Recent experiments have implemented basic ingredients for observing topological phases such as synthetic magnetic fluxes,[121,122] discussed further in Sec. VIII. One advantage compared to optical cavities is the greater flexibility in lattice designs; for example, individual resonators can be stretched or bent without affecting their tight binding model properties, enabling the implementation of exotic lattices, e.g., embedded in hyperbolic space.[123]

F. Electronic circuits

Electronic circuits have recently emerged as a convenient and accessible platform for studying the combination of nonlinearity with band topology.[14,71,72,101,124–130] Key advantages include the ease with which such circuits can be designed and fabricated using circuit simulators, printed circuit boards (PCBs), and other commodity technologies; the fact that they can be characterized using inexpensive laboratory equipment such as function generators and oscilloscopes; the availability of strongly nonlinear circuit elements; and the exciting prospect of using circuit wiring to implement complex geometries (like Möbius strips[71]) that are practically impossible to realize on other platforms. Such systems include circuits implemented on breadboards or PCBs, typically operating in the 0.1–500 MHz frequency range,[14,71,101,127–130] as well as electromagnetic structures (such as microstrip resonator arrays) with attached lumped circuit elements, which can operate at GHz frequencies.[72]

The most commonly used method for introducing nonlinearity into an LC circuit is to use varactor diodes.[14,101,129,130] These two-port circuit elements are essentially diodes operated in reverse bias; with increasing reverse bias voltage, the thickness of the diode's depletion region increases and its effective capacitance decreases. For alternating-current (AC) operation, a nonlinear capacitor can be implemented by a pair of varactors arranged back-to-back, such that neither varactor can be forward-biased. The resulting capacitance decreases with the magnitude of the voltage across the circuit element, independent of its sign.

While back-to-back varactors have the advantage of realizing an extremely simple Kerr-like nonlinearity, they are not the only nonlinear circuit elements available. The alternatives, however, introduce an additional complication: they are typically not only nonlinear but also "active" (i.e., energy-non-conserving or non-Hermitian). As we will discuss in Sec. VI, the combination of

nonlinearity, non-Hermiticity, and band topology to form topological lasers is an active and largely unsettled area of research, and electronic circuits may serve as a key playground for future experimental investigations. Recently, Kotwal et al. have taken the first steps in this direction by performing a theoretical analysis of 1D and 2D topological circuits with nonlinear negative-resistance elements such as van der Pol circuits or tunnel diodes.[131] They uncovered an extremely rich set of behaviors, such as SSH-like boundary states that exhibit self-sustained limit cycle oscillations, which can induce synchronized bulk oscillations that mediate the interactions between different boundaries.

G. Mechanical metamaterials

Finally, we mention related experiments based on the platform of mechanical metamaterials. Although, strictly speaking, not photonics, similar governing equations make this a useful setting for investigating nonlinear topological phenomena. The first mechanical implementation of the quantum spin-Hall effect (QSHE) was experimentally demonstrated by Süsstrunk and Huber[132] in a lattice of mechanical pendula, with operating frequency in the Hz range. Based on this model, nonlinear Duffing oscillators connected by linear springs can support unidirectional nonlinear traveling edge waves.[133] Another nonlinear topological phononic crystal—a 1D array which consists of masses connected with two alternating types of nonlinear springs—was analyzed in Ref. 134. It was numerically shown that by increasing the excitation amplitude the lattice makes a topological transition giving rise to different families of nonlinear solutions.

V. LOCALIZED NONLINEAR STATES
A. Motivation and general approaches

Nonlinear generalizations of linear topological models support peculiar mechanisms for the field localization, leading to phenomena such as topological gap solitons and nonlinear edge states (bulk and edge solitons),[135–138] embedded solitons,[139] and semi-vortex solitons,[140] as depicted in Fig. 6. Notably, these solitons have nontrivial vorticity and a pseudospin structure. Interestingly, in many cases, the formation of topological solitons can be understood in terms of the nonlinearity locally inducing a domain wall between different topological phases, with the soliton being self-consistently trapped by the interface. Since what matters is a change in the topological invariant across the interface,[140] one can obtain solitons that create a trivial defect within a nontrivial phase,[135] as well as solitons that create nontrivial defects out of trivial phases.[139]

These phenomena pose an interesting challenge to our understanding of band topology. Strictly speaking, the concept of band topology is tied to linearity, which is necessary for the existence of a Bloch Hamiltonian and band structure, as discussed in Sec. III. Some authors have explored correcting the definition of the Berry phase in order to describe the band structures of weakly nonlinear Bloch modes with fixed homogeneous intensities.[141,142] However, localized nonlinear states—solitons—represent strong modifications to an underlying topological structure, or even the creation of topological order from a trivial system.

From a practical point of view, localized nonlinear states may be extremely useful for tunable topological photonics.[9,99,137,143] They may also be accompanied by novel effects such as the spontaneous

breakdown of Lorentz reciprocity, wherein the light intensity itself determines whether the light can propagate via an edge state.[134,144]

In lattice models, nonlinearity can be introduced either into the on-site energy or the coupling between lattice sites. The resulting behavior may be non-universal, sensitive to either the form of the nonlinearity or the particular lattice geometry. For weak nonlinearities, the formation of edge solitons was understood in the traditional framework of scalar effective nonlinear Schrödinger equations, where the nonlinearity compensates the linear edge state dispersion.[146,149,150]

For stronger, non-perturbative nonlinear phenomena, exact solutions are scarce, and they require a combination of approximate approaches such as the variational method, analytical solutions in simple limits, and numerical solutions of specific lattices.[7,97,136,139,145] For example, the self-induced traveling edge states of Ref. 139 were first obtained analytically in the special limit where they are perfectly localized to a single lattice site. This exact solution was then used as an initial guess for numerics to demonstrate their persistence over a broader range of parameters, as shown in Fig. 6(b).

Further insights can be obtained using the continuum nonlinear Dirac model, through the perspective of phase portraits and bifurcation analysis. This approach is able to describe bulk solitons and nonlinear edge states in a variety of 1D and 2D nonlinear photonic lattices, including SSH, honeycomb, and Kagome lattices. For instance, treating $\hat{H}_D$ in Eq. (2) as an operator, which contains spatial derivatives, and incorporating nonlinear corrections as a field-dependent operator $\hat{H}_{NL}$ yield a nonlinear equation for the evolution of the spinor wavefunction $\mathbf{\Psi} = [\Psi_1, \Psi_2]$,

$$i\partial_t \mathbf{\Psi} = (\hat{H}_D(\delta\mathbf{k}) + \hat{H}_{NL})\mathbf{\Psi}. \qquad (8)$$

This can be tackled analytically for various types of nonlinearity, including the one most commonly encountered in optics, a local cubic nonlinearity of the form $\hat{H}_{NL} = -g[|\Psi_1|^2, 0; 0, |\Psi_2|^2]$. By contrast to relativistic field theory, nonlinear Dirac equations in photonics appear as effective equations and they are not restricted by the Lorentz invariance. As compared to the nonlinear Schrödinger equation, the existence and stability analysis of solitons in Dirac models is more subtle because of the absence of the rigorous Vakhitov–Kolokolov criterion.[151–153]

B. Su–Schrieffer–Heeger lattices

The simplest structure linking topology and nonlinearity is a nonlinear version of the 1D SSH model. Such a model can be implemented in arrays of resonant elements with nonlinear couplings.[144,154] This formally corresponds to off diagonal nonlinearity in Eq. (8). The model exhibits a self-induced topological transition, in which the nonlinearity drives the lattice into a different topological phase supporting edge states. However, the resulting nonlinear edge states are not truly localized as they sit on a nonzero intensity background.

This model is challenging to realize in optics, where local on-site Kerr nonlinearities are more feasible, but has been implemented in electronic circuits by Hadad et al.[101] The nonlinear SSH circuit was created using a dimerized 1D lattice of LC resonators with two resonators (sites) per unit cell, shown in Fig. 7(a). The intra-cell and inter-cell couplings were implemented by two types of capacitors, one of which was nonlinear [Fig. 7(b)]. The self-induced edge state was
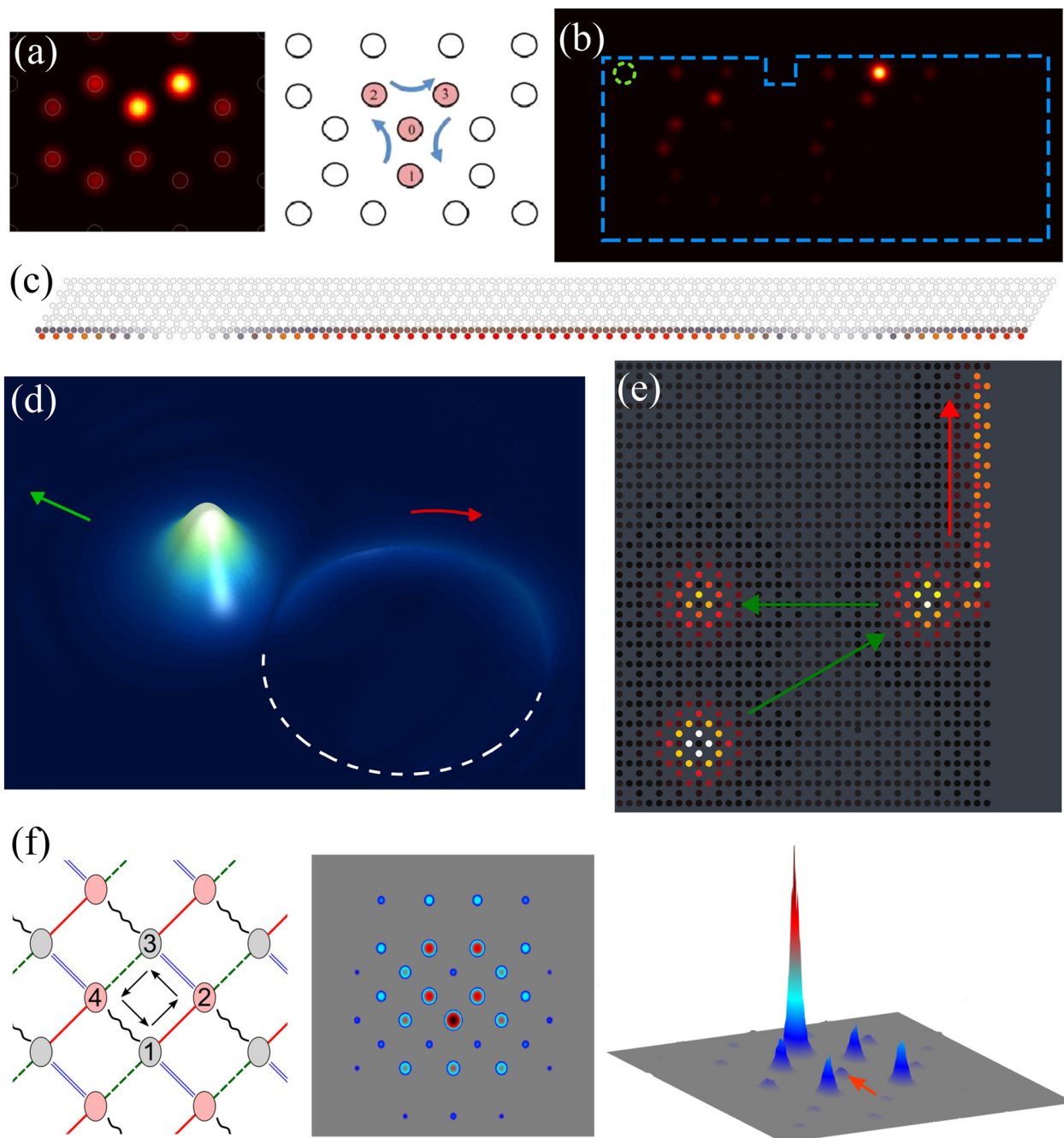
FIG. 6. Solitons localized in topological lattices. (a) Bulk soliton in a honeycomb lattice of helical waveguides alongside a sketch of the intraperiod rotation of the intensity.[145] The wavepacket rotates around the nonlinearity-induced defect as an edge state in a clockwise direction. (b) Single-site localized edge soliton propagating unidirectionally along the edge of the Floquet lattice of coupled helical waveguides embedded in a medium with local Kerr nonlinearity.[139] Shown is a numerically calculated profile of the output intensity after propagation around a missing edge waveguide, when the waveguide circled in green is excited at the input. (c) Dark (left) and gray (right) edge solitons (seen as whitened dips in intensity) at the boundary of a Kagome lattice strip of coupled microcavity pillars.[146] In the weakly nonlinear regime, the solitons in the exciton–polariton condensate are constructed from wavepackets of topological edge modes with the envelope described by the Schrödinger equation. [(d) and (e)] Excitation of chiral topological edge modes by scattered traveling gap solitons at (d) domain walls created by mass inversion in a 2D continuum Dirac model;[137] (e) at the pointy edge of the Lieb lattice.[147] (f) Observation of topological gap solitons in a square lattice of helical waveguides femtosecond-laser-written in a borosilicate glass:[148] schematic of the lattice (left); calculated intensity profile of the soliton whose maximum exhibits cyclotron-like rotation jumping four sites (1–4) sequentially (middle); measured output intensity distribution (right) at a propagation distance of 1.5 driving period for an input power of 3.32 mW.
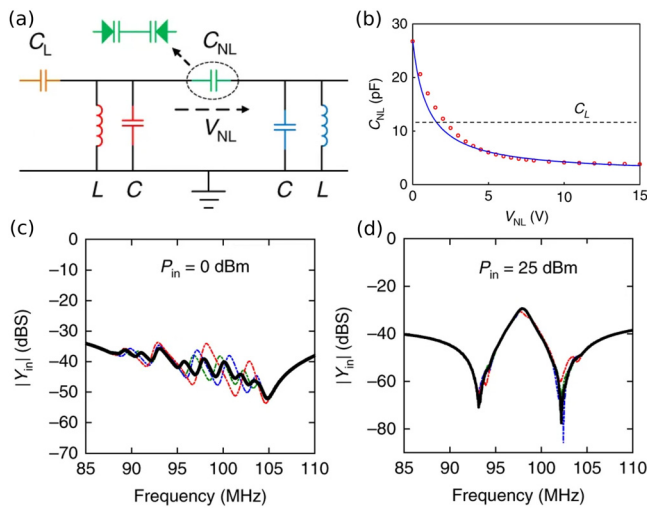
FIG. 7. Nonlinear electronic circuit analog of the Su–Schrieffer–Heeger model.[101] (a) Schematic of the unit cell consisting of sites (LC resonators) coupled via linear C_L and nonlinear C_{NL} capacitors. (b) Nonlinear capacitance C_{NL} implemented using back-to-back varactor diodes. [(c) and (d)] Measured input admittance spectra at the edge of a 6-cell chain. (c) In the linear limit, the chain is trivial and multiple peaks (resonances) associated with bulk modes are observed. (d) In the nonlinear regime a self-induced edge state emerges, visible as a single dominant resonance in the middle of the spectrum. A solid black line corresponds to an ideal chain while thin colored curves are measured spectra in the presence of various defects, demonstrating robustness to disorder. Adapted with permission from Hadad et al., Nat. Electron. **1**, 178–182 (2018). Copyright 2018 Nature Springer.

indeed observed in the circuit experiment, in the form of an input admittance peak appearing at a mid-gap frequency when the lattice was driven above a threshold power level, as shown in Figs. 7(c) and 7(d). The resonance frequency was shown to be insensitive to disorder introduced by deliberately shorting different resonators to ground, consistent with the topological protection in the underlying linear SSH model.

A few experiments have now probed SSH models with on-site Kerr nonlinearity.[99,107] In particular, Dobrykh et al. demonstrated nonlinearity-induced tuning of the linear topological edge states in an array of coupled nonlinear microwave resonators.[99] The SSH array was made of $N = 7$ broadside-coupled split-ring resonators with the magnetic dipole resonance at the frequency $f_0 \approx 1.5$ GHz. The Kerr-type nonlinear tunability of the frequency was introduced by varactor diodes mounted inside the gap of each split ring resonator. The experiment was conducted in the pump-probe setup, where a homogeneous pump tuned to the linear edge state frequency was used to excite the array, and the probe measures the spectrum of fluctuations about the resulting nonlinear steady state. The setup can be described by the nonlinear lattice model

$$\frac{da_n}{dt} = -\gamma a_n - i|a_n|^2 a_n + t_{n,-}a_{n-1} + t_{n,+}a_{n+1} + P, \quad (9)$$

where a_n is a normalized amplitude of the n-th oscillator ($n = 1, \ldots, N$), γ is a damping coefficient, P is an amplitude of the resonant homogeneous pump, and $t_{n,-}$, $t_{n,+}$ are alternating weak and strong nearest-neighbor couplings. With increasing the power, the

field becomes localized at the edge and induces a nonlinear blue shift for the edge state, as shown in Fig. 8.

Bulk solitons and edge states in SSH models with on-site Kerr nonlinearity have been also analyzed theoretically from different perspectives.[136,137] Bulk solitons exhibit anistropic pseudospin (sublattice) textures, which results in asymmetric interactions with localized defects.[136] Later, Ref. 137 showed that the bulk solitons and nonlinear edge states in this setting have a closely related origin; mutual transformations between edge and bulk states, forbidden in linear limit, can occur in the nonlinear regime. It has also been predicted that traveling bulk solitons are capable of exciting the edge states by reflecting off the topologically nontrivial edge.[137,147] In this regard, recent experiments using coupled optical fiber loops have demonstrated coupling between localized topological edge states and nonlinear bulk modes.[107]

C. Two-dimensional lattices

Theoretical studies of 2D nonlinear topological lattice models have revealed several interesting new phenomena inaccessible in 1D settings: bulk solitons exhibit cyclotron-like rotation or vorticity[140,145] and under an applied force experience anomalous Berry curvature-induced transverse shifts.[147] Self-induced edge solitons can be mobile, traveling along the edge and around corners and certain defects.[6,139] These models are, however, more challenging to implement in optics experiments. For instance, using longitudinally modulated waveguide arrays, it is relatively easy to create topological lattices, but the longitudinal modulation induces additional radiation losses reducing already weak nonlinear effects.[135,139,145] On the other hand, nonlinearities are
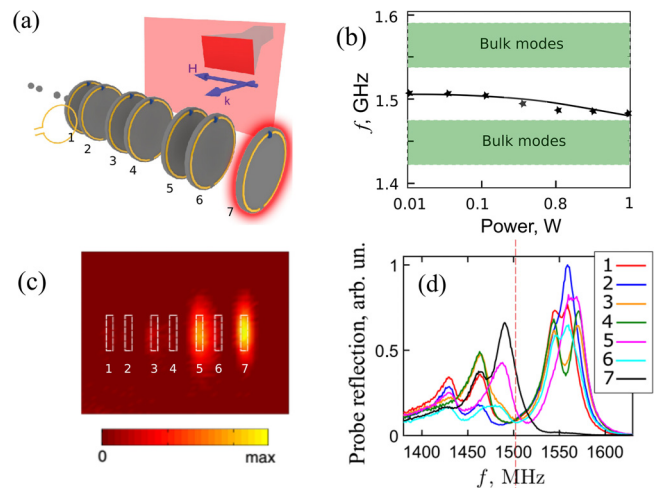
FIG. 8. Nonlinear tuning of microwave topological edge states.[99] (a) Experimental setup: SSH array of nonlinear microwave resonators with source (horn antenna) and receiver (loop antenna). (b) Measured nonlinear shift of the edge state frequency depending on the pump power. With increasing the pump power, the edge state frequency is gradually blue-shifted from the mid-gap. (c) Measured magnetic field distribution for weak pump exhibits a staggered profile characteristic of the linear SSH model. (d) Spatially resolved pump–probe reflection spectrum for power 0.8 W. Curves 1–7 correspond to the resonators from left to right. The central peak in the black curve, corresponding to the excitation of the edge resonator, is detuned from the linear mid-gap position marked by a dashed vertical line.

easier to observe using exciton–polaritons, but strong external magnetic fields are required to create a topological bandgap.[7,136,138,146,150,155,156]

Zangeneh-Nejad and Fleury[130] have implemented nonlinear circuits generalizing the SSH model to a class of high-order topological insulators.[44,127,129] The 2D lattice they studied hosts a nontrivial topological phase characterized by quantized Wannier centers (with quantized values of the bulk polarization) and robust mid-gap corner modes,[157] with the topological transition governed by the ratio of intra-cell to inter-cell couplings, similar to the SSH case. The nonlinear circuit was again implemented by using back-to-back varactors for the inter-cell connections, and self-induced corner states were observed above a certain power threshold.

Very recently, the observation of topological gap solitons has been reported in a square lattice of laser-written periodically modulated waveguides, which creates a Floquet topological phase. The nonlinearity arises from the optical Kerr effect of the ambient glass. Under the paraxial approximation, the z propagation of light through this photonic lattice is captured by the discrete equation, which includes the linear tight-binding Hamiltonian with nearest-neighbor evanescent coupling and diagonal on-site nonlinearity,

$$i\frac{\partial a_n}{\partial z} = \sum_{\langle n'\rangle} H_{nn'}(z)a_{n'} - |a_n|^2 a_n. \tag{10}$$

In the nonlinear dispersion given by the dependence of quasienergy (propagation constant) on power, a family of gap solitons bifurcates from the linear modes and shows maximal localization in the vicinity the mid-gap quasienergy. In accordance with their chiral nature, solitons residing in the topological bandgap exhibit continuous cyclotron-like rotation. The solitons were probed in propagation using single-site excitation in the input [see Fig. 6(f)]. The characteristic peak in the degree of localization vs power was observed that distinguishes topological gap solitons from trivial solitons in static lattices of straight waveguides, where localization continuously grows up and then saturates at very high nonlinearity.[148]

D. Future directions

The initial studies of two-dimensional topological solitons have largely focused on models of the QH phase, in which time-reversal symmetry is explicitly broken, and topological phases are well-defined even in the absence of special symmetries. While this aids in the interpretation of the solitons as nonlinearity-induced domain walls, these models are more challenging to realize in experiment. There have now been many experimental demonstrations of time-reversal symmetric QSH and VH phases using nanophotonic crystals supporting tight light confinement and appreciable Kerr nonlinearities.[66,67,69,158] Recent realizations of honeycomb lattices in nonlinear atomic vapors are also a promising step toward observing self-localized states in these models.[82,97] Studies of self-localized states in time-reversal symmetric topological models remain relatively scarce, however, and form an interesting direction for further research. For example, Bleu et al.[159] have predicted robust, charge-controlled transport of vortex solitons along VH domain walls.

VI. TOPOLOGICAL LASERS
A. Motivation and general approaches

Topological photonics has potential applications for the design of lasers, as it provides a systematic way to control the number and

degree of localization of spectrally isolated edge and defect modes in photonic structures. For example, mid-gap modes of 1D topological lattices are optimally localized within the bandgap, which allows for the tight confinement of lasing modes.[94,160–163] In 2D systems, backscattering-immune edge modes hold promise for the design of ring cavities supporting large modal volumes and single mode operation regardless of the cavity shape.[8,53,164] In both cases, the resulting modes are protected against certain classes of fabrication disorder, offering improved device reliability.

At a fundamental level, topological lasers are interesting as a platform for exploring the interplay between nonlinearity and topology. Once a mode rises above the lasing threshold, it becomes crucial to account for nonlinear gain saturation, which is what enables the system to relax toward a steady state. The high optical intensity within the laser cavity can also lead to other nonlinear effects such as Kerr self-focusing. Nonlinearities in conventional lasers are known to lead to a rich variety of phenomena including chaos and instabilities, so it is interesting to ask how these effects interact with the topological features of the photonic structure.

Since 2017, several experiments have demonstrated lasing of topological edge modes in both 1D and 2D lattices. The experiments can be divided into two classes: (1) photonic lattices of coupled resonators with structural periods somewhat larger than the operating wavelength, and (2) photonic crystals with structural periods comparable to the operating wavelength. These systems have been modeled as either class A or class B lasers.[165]

In class A lasers such as quantum cascade lasers, the photon lifetime is much longer the gain medium's polarization and population inversion, which are adiabatically eliminated leaving a nonlinear wave equation involving only the optical field amplitude ψ. Under the tight binding approximation, this results in a discrete set of equations of the form

$$i\partial_t\psi_n = \hat{H}_L\psi_n + \frac{g_n(i+\alpha)}{1+|\psi_n|^2/I_{\text{sat}}}\psi_n, \tag{11}$$

where n indexes the weakly coupled resonators forming the tight binding lattice and $\hat{H}_L$ is an effective Hamiltonian accounting for all the linear effects such as absorption γ, coupling between the resonators J, and disorder W. The second term is nonlinear and describes the saturation of the gain induced by the pump g_n, governed by a characteristic intensity scale I_{sat}. The linewidth enhancement factor α accounts for carrier-induced shifts of the ambient refractive index, which can lead to self-focusing or defocusing behavior. This model assumes frequency independent gain, a good approximation for tight binding lattices which typically have a narrow bandwidth.

Semiconductor gain media such as quantum dots that are typically integrated with photonic nanostructures are class B lasers. In these lasers, the free carriers providing the gain have a much longer lifetime than the photons and their dynamics must be taken into account, resulting in coupled equations of the form[166,167]

$$i\partial_t\psi_n = \hat{H}_L\psi_n + N_n(i+\alpha)\psi_n, \tag{12}$$

$$\tau\partial_t N_n = R_n - N_n - (1+2N_n)|\psi_n|^2, \tag{13}$$

where $N_n(t)$ is the normalized excess carrier population, R_n is the normalized excess pump rate, and τ is the ratio between the carrier and

photon lifetimes ($\approx$100–1000 for semiconductor lasers and $\ll$ 1 for class A lasers). A significant challenge presented by class B models is that while topological protection can be readily implemented in the photonic part of the field, the carrier populations N_n are not coupled directly to one another and do not share this protection. Slow carrier dynamics are a well-established source of instabilities in coupled semiconductor laser arrays; as the carrier lifetime is increased, the stable steady states of the class A limit become unstable and are replaced by limit cycles and eventually chaotic dynamics.[165]

In both classes of lasers, the lasing modes can be obtained numerically using standard iterative methods to solve for stationary states of nonlinear wave equations (e.g., Newton's method) and seeking real frequency solutions. The initial guess for these iterative schemes is typically chosen to be the profile of the mode of interest at its threshold, obtained by solving a linear eigenvalue problem, followed by standard linear stability analysis to determine if the lasing modes are stable. The solution can be further verified by taking a direct numerical solution of the governing equations starting from small random field amplitudes as the initial condition; this can result in convergence to the stationary solution (in the case of stable single mode lasing), persistent oscillations between competing lasing modes (multimode lasing), or more complex dynamics such as irregular pulsations and chaos.[165]

B. Lasing of 1D edge modes

The first examples of topological lasers were based on the 1D Su–Schrieffer–Heeger (SSH) model. Interest in this type of topological laser was sparked by a 2013 theoretical study of the SSH model with staggered linear gain and loss,[168] which modeled a 1D topological photonic crystal under inhomogeneous pumping. For sufficiently weak gain/loss, the bulk modes overlap with both the gain and loss regions due to the chiral symmetry of the SSH model. This results in bulk modes with vanishing net gain. At the ends of the array or at domain walls, there exist topological modes localized to a single sublattice; pumping this sublattice gives the modes nonzero net gain, allowing them to lase before the bulk modes. The topological modes inherit a certain robustness to disorder, since they reside in the middle of the bandgap and are spectrally isolated from other modes. As the gain/loss is increased, the bulk bandgap becomes smaller and eventually closes. The bulk modes then start to localize onto the pumped sublattice and compete with the topological modes, resulting in multiple modes rising above the lasing threshold.[169]

These predictions were observed in a trio of photonic lattice experiments in 2017.[160–162] St.-Jean et al.[160] employed a zigzag polariton lattice of micropillars, while both Parto et al.[161] and Zhao et al.[162] used ring resonator lattices with embedded InGaAsP/InP quantum wells as the gain medium. The latter is illustrated in Fig. 9(a). Uniform pumping results in spatially delocalized multimode emission due to competition between bulk modes, while pumping a single sublattice results in single mode lasing of the topological interface state as the bulk bandgap remains open. Robustness of the edge modes to certain classes of perturbations was also demonstrated.

Second generation designs based on nanoscale photonic crystals are now emerging. In 2018, Ota et al. reported lasing at $\lambda \approx 1040$ nm in a protected defect mode at a topological domain wall of a GaAs nanobeam photonic crystal with embedded InAs quantum dots,[94] shown in Fig. 9(b). Their design supports strongly confined defect modes with modal volumes as small as $0.23(\lambda/n)^3$, quality factors up
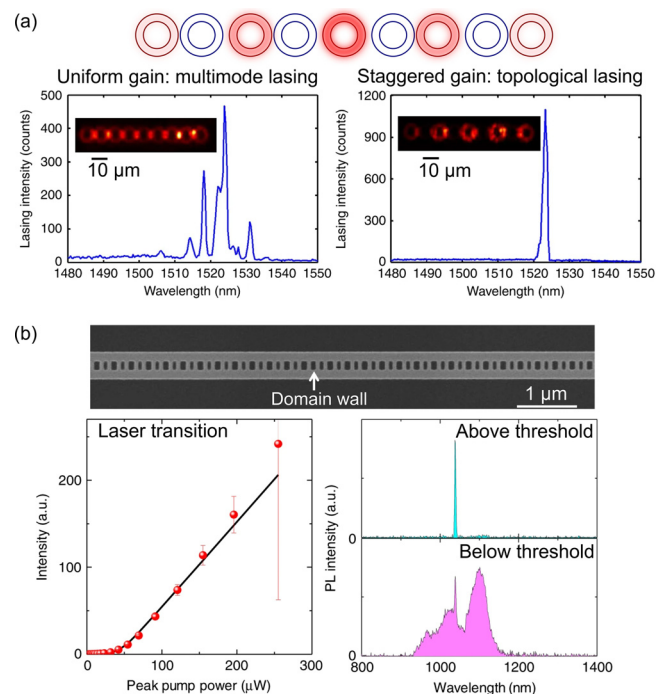

FIG. 9. Topological lasers based on the 1D Su–Schrieffer–Heeger chain. (a) Photonic lattice of coupled silicon microring resonators exhibiting multimode or single mode lasing depending on the gain profile.[162] (b) Lasing at a topological domain wall in a GaAs nanobeam photonic crystal.[94] Left panel: emission intensity vs pump power showing a transition to lasing at the threshold power of about 46 μW. Top right: narrow spectral line of the topological mode emission above the threshold at the pump power 150 μW. Bottom right: broad spectrum of the emission below the threshold at the pump power 5 μW. Adapted with permission from Zhao et al., Nat. Commun. **9**, 981 (2018). Copyright 2018 Author(s), licensed under a Creative Commons Attribution 4.0 License; Ota et al., Commun. Phys. **1**, 86 (2018). Copyright 2018 Author(s), licensed under a Creative Commons Attribution 4.0 License.

to $Q \approx 59\,700$, and spontaneous emission coupling factor $\beta \sim 0.03$. Similarly, Han et al.[163] used nanocavities based on L3 defects in a hexagonal InAsP/InP photonic crystal to achieve $Q \approx 35\,000$ and $\beta \approx 0.15$ at 1550 nm. These values are, however, comparable to conventional photonic crystal cavities; the main benefit of the topological design is the ability to systematically control the Q factor and mode volume via the size of the bulk bandgap while preserving single mode operation. So far, these experiments have been limited to optical pumping by ultrashort pulses at powers relatively close to the lasing threshold, with observations largely explained in terms of linear modes.

The SSH model also provides a simple testbed for exploring nonlinear dynamics of topological lasers and understanding whether there can be meaningful topological effects in the nonlinear regime. For example, if the linewidth enhancement factor is neglected ($\alpha = 0$), under inhomogeneous pumping the SSH model exhibits a dynamical charge conjugation symmetry, a nonlinear and non-Hermitian analog of the chiral symmetry protecting the linear topological edge states.[170] The charge conjugation symmetry protects stationary zero modes

localized to the pumped sublattice, with the number of these modes only changing at nonlinear bifurcations, which can be considered a nonlinear topological transition.[171] Above a critical power, the zero modes become unstable and give birth to symmetry-protected time-periodic oscillatory modes at Hopf bifurcations. While $\alpha \neq 0$ breaks the charge conjugation symmetry, the spectral isolation of the nonlinear modes means that they can persist for sufficiently weak symmetry-breaking perturbations. Similar behavior is observed for other forms of nonlinearity[172] and in 2D analogs of the SSH model such as the Lieb lattice.[171]

The SSH model can also form the basis for a class of topology-inspired large volume single mode lasers by introducing *non-Hermitian coupling*. For example, asymmetric non-Hermitian coupling $J_{n,n\pm1} \propto \exp(\pm h)$ describes the preferential hopping of the optical field from site n to $n+1$, equivalent to an imaginary effective gauge field h. In a finite lattice, this does not affect the energy spectrum because the gauge field can be removed by the gauge transformation $\psi_n \rightarrow \psi_n \exp(hn)$. However, this transformation changes the eigenmodes' localization: all modes start to localize to one end of the lattice. When edge states exist (e.g., in the SSH model), the non-Hermitian localization competes with the localization ξ of the topologically protected edge states. At a critical imaginary gauge field strength $h = \xi$, this leaves all but one of the modes localized to one edge of the system, with the remaining (topologically protected) zero mode delocalized over the whole lattice and therefore able to saturate the gain at all the pumped sites.[173]

The (Hermitian) SSH model is not the only way to design novel topological lasers. More recently, the idea of non-Hermitian topological phases has been developed,[174] which can be used to design disorder-robust delocalized modes in 1D systems using non-Hermitian coupling. As a second example, symmetric non-Hermitian coupling $J_{n,n\pm1} \propto e^{ih}$ describes effective gain dependent on the modal wavenumber, i.e., the relative phase between the optical field at neighboring lattice sites.[166,167] This phase-dependent gain can promote single mode lasing in simple quasi-1D ring-shaped lattices. Another recent proposal by Longhi[175] has predicted a non-Hermitian topological transition from single mode lasing to multi-mode lasing in a mode-locked laser.

C. Lasing from 2D edge modes

The first experimental demonstration of lasing of 2D topological edge states by Bahari *et al.* in 2017[53] used a photonic crystal embedded on a yttrium iron garnet (YIG) substrate, shown in Fig. 10(a). Breaking time reversal symmetry via the magneto-optic effect creates a Chern insulator phase with a bandgap hosting protected chiral edge modes. Despite the resulting topological bandgap (42 pm) being very small due to weakness of magneto-optical effects at the operating wavelength 1530 nm, as well as the entire device being pumped, the lasing profile shown in Fig. 10(b) is strongly localized to the edge and insensitive to its shape. This unexpected observation still awaits a theoretical explanation: based on the behavior of the 1D SSH model and 2D lattices, uniform pumping should have led to multi-mode lasing of bulk modes unless the gain medium has a narrow bandwidth centered on a topological bandgap.[176] In a follow-up study, the same group demonstrated the generation of high charge ($|l| \sim 100$) optical vortex beams using circular-shaped topological domain walls.[177]

Around the same time, Harari *et al.*[178] studied theoretically class A laser models of 2D optical ring resonator lattices exhibiting

topological edge states. They found that a pump localized to the edge sites was required to suppress bulk mode lasing and induce stable single mode lasing of the edge states. This single mode lasing also persisted in the presence of moderate disorder and weak symmetry-breaking perturbations that spoil the topological protection in the linear regime. In comparison, in similar non-topological models, disorder tends to induce mode localization, resulting in multi-mode lasing involving modes localized at different positions along the edge. Ring resonator lattices incorporating gain and lasing of the topological edge states were then realized by Bandres *et al.*;[8] see Figs. 10(c) and 10(d). Interestingly, the combination of nonlinear gain saturation with spatial asymmetry (induced by either asymmetric pumping, or incorporating S bends into the ring resonators) resulted in observable optical non-reciprocity: preferential lasing of a single mode handedness or chirality, even though the underlying structure is non-magnetic and respects time-reversal symmetry, meaning that the linear edge modes occur in counter-propagating pairs with opposite spin. This is visible in Fig. 10(d) as an imbalance between the intensities at the two output ports.

Another 2D experiment was based on a honeycomb lattice for exciton–polaritons combined with a strong magnetic field.[164] The spin–orbit coupling of the polariton condensate combined with a magnetic field-induced Zeeman shift created a Chern insulator phase, although the resulting bandgap was small, making it difficult to observe strong localization of the edge states. A subsequent theoretical study by Kartashov and Skryabin[179] of the governing class A gain model verified the existence of stable nonlinear lasing modes in this platform. They additionally found that above the polariton lasing threshold, self-action terms such as α lead to frequency shifts of the edge modes toward the bulk band edge. As the lasing mode approaches the band edge, dynamical instabilities first develop, and then at higher powers, the edge mode delocalizes due to resonance with bulk modes. Thus, the topological protection of the edge state lasing mode does not persist in the nonlinear regime. A more involved and accurate model of a polariton condensate would, however, incorporate a rate equation for the exciton reservoir density.[180]

In class B models, the slow carrier dynamics are another source of instability.[166] While the photonic field remains localized to the edge and protected against disorder-induced backscattering, due to the carrier dynamics a limit cycle forms rather than a stationary state. In this limit cycle, a localized excitation circulates around the edge of the array due to competition between different edge modes with slightly different energies and similar effective gain. Because of the slow carrier response, the "winner takes all" effect of the saturable gain in the class A laser is not available to strictly enforce single mode operation. Due to this mode competition, the details of the dynamics and emission spectra become sensitive to the particular disorder realization.

Finally, we mention very recent theoretical studies of topological laser models analyzing the effects of initial and time-dependent noise on the edge mode lasing,[181] its spatial and temporal coherence,[182] and the transition from class A to class B lasing by varying the carrier lifetime.[183] The precise energy of the lasing mode selected from one of the topological edge states spanning the gap is sensitive to initial fluctuations, due to similar gain of edge modes close to the middle of the bandgap. Large arrays exhibit the well-known Kardar–Parisi–Zhang scaling of their correlations, but always with reduced coherence compared to the single mode Schawlow–Townes linewidth. Many of these features can be captured by simpler one-dimensional effective models
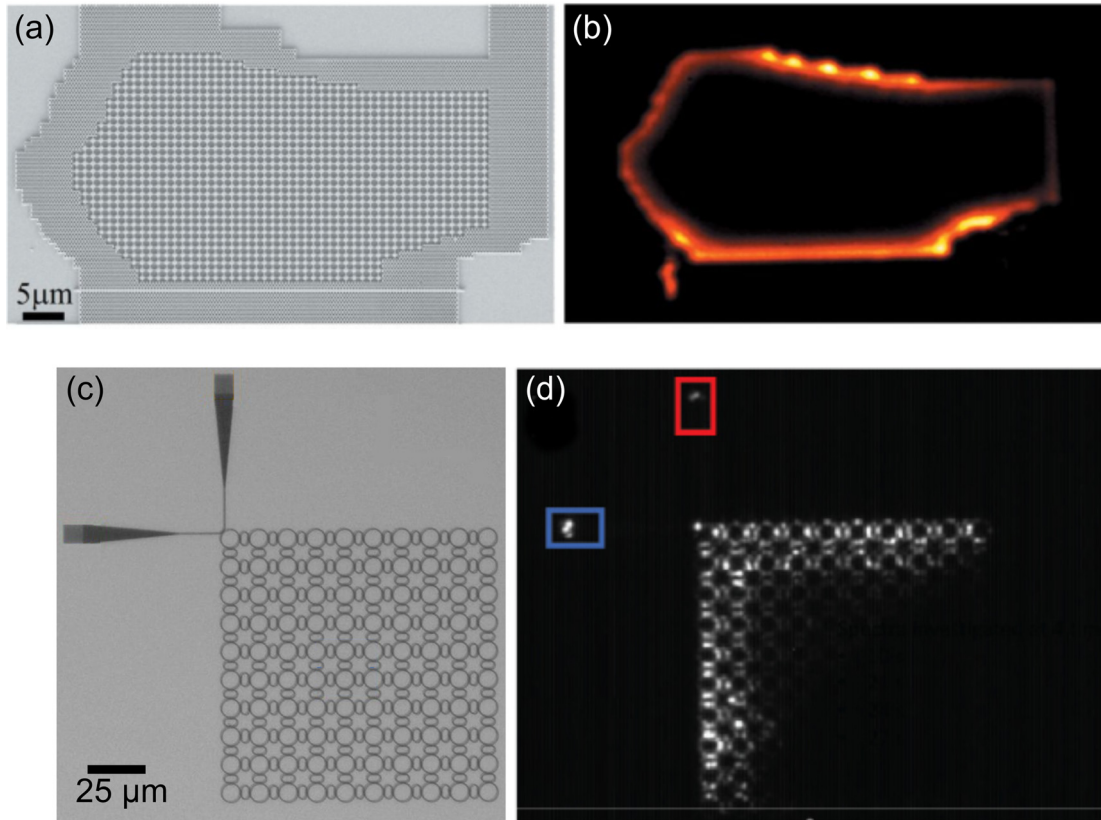
FIG. 10. 2D topological lasers on photonic edge states. Top row: [(a) and (b)] InGaAsP/YIG photonic crystal laser.[53] (a) InGaAsP photonic crystal bonded on gyrotropic yttrium iron garnet (YIG). Under an external magnetic field, the inner domain forms a Chern insulator. (b) Intensity profile of the chiral lasing edge mode at the wavelength 1064 nm. Bottom row: [(c) and (d)] InGaAsP ring resonators laser.[8] (c) Photonic lattice of coupled InGaAsP microring resonators exhibiting spin momentum-locked edge states; (d) Chiral lasing via asymmetric pump: Despite preservation of time reversal symmetry, asymmetric pumping induces chiral lasing due to nonlinear gain saturation, resulting in an imbalance in intensity from the output ports coupled to the two spin states (highlighted in red and blue). Adapted with permission from Bahari *et al.*, Science **358**, 636–640 (2017). Copyright 2017 The American Association for the Advancement of Science; Bandres *et al.*, Science **359**, eaar4005 (2018). Copyright 2018 The American Association for the Advancement of Science.

describing the edge states.[182,183] The advantage of the 2D topological edge state lasers is that their coherence remains robust to (and can even be enhanced by) moderate static disorder, compared to conventional 1D arrays which form multiple incoherent lasing modes localized by disorder.

D. Future directions

It is of interest to extend topological lasers to other gain media and material platforms, such as waveguide or fiber loops.[184] For example, lasing in 2D honeycomb and square lattices of plasmonic nanoparticles using organic dyes as the gain medium was recently demonstrated in Refs. 83 and 185. Such class A lasers can avoid instabilities due to slow carrier dynamics. The radiative coupling present in such plasmonic systems means that the tight binding approximation is no longer valid, requiring re-examination of the results discussed above.

Most studies to date have focused on lasing at the edges of finite systems, but there is now growing interest in alternative schemes based on lasing in the bulk of extended topological lattices, using one-dimensional topological domain walls of VH or QSH lattices[186–189] and point-like topological defects.[190] The topological modes of the VH models lie below the light line, such that the lasing modes are confined in the plane of the photonic crystal.[187,189] On the other hand, the QSH models and point-like defects act as vertical cavity surface emitting lasers.[186,189,190]

The main selling point of topological lasers to date has been their potential for robust single mode continuous wave lasing, but for applications such as frequency comb generation or ultrashort pulse generation robust multimode emission is required. This can be achieved using lattices hosting multiple topological gaps and edge states,[191] or by employing synthetic dimensions.[192]

The first topological lasers realized in experiment were proofs of concept based on optically pumped gain media. Any real device applications will require electrical pumping, analysis of effects such as modulation bandwidth and how to avoid the instabilities discussed above,[165] and most importantly, a "killer application" in which topological lasers outperform their conventional counterparts, such as

tolerance to fabrication imperfections. As a step in this direction, Suchomel *et al.*[193] have implemented electrically pumped polariton lasers in artificial honeycomb and square lattices, which can be readily generalized to topological lattices such as the time reversal-symmetric shrunken-expanded hexagon or VH designs discussed in Sec. III. Very recently, Zeng *et al.* realized an electrically pumped quantum cascade laser based on the VH edge states.[194]

VII. FREQUENCY CONVERSION
A. Motivation and general approaches

Topological photonics offers potential advantages for frequency conversion applications. First, the conversion rate depends on the local pump amplitude or intensity (in quadratic or cubic nonlinear media, respectively) and can be enhanced when the pump excites a strongly localized topological edge mode. Second, it is usually necessary to filter the weak generated signal from the much stronger pump beam; this filtering can be facilitated by the co-existence of bulk and edge modes with very different spatial profiles, as well as the ability to robustly control the propagation direction of edge modes occupying different bandgaps. Finally, phase-sensitive nonlinear wave mixing processes provide a novel all-optical mechanism to tune the topological properties of small amplitude signal beams.

B. Harmonic generation

The first observation of topologically enhanced harmonic generation was carried out using a small zigzag array of silicon nanodisks fabricated on a glass substrate.[11] The zigzag array implements a variation of the SSH model based on alternating strong and weak dipole–dipole couplings, with the topological phase controlled by the zigzag angle, as shown in Fig. 11. Due to intrinsic nonlinearity of silicon, topological edge states facilitate resonant generation of third-harmonic radiation. The topology-driven third-harmonic signal was shown to be robust against coupling disorder due to misalignment of the individual nanodisks; a number of arrays with randomly generated bond angles between the disks were fabricated, and in full agreement with theory, for disorder angle less than a critical value of 20°, edge states were observed. Remarkably, the observed third-harmonic radiation switched from one edge of the array to the other one, depending whether the system was illumination from the substrate or from air. This asymmetric harmonic generation is a type of nonreciprocal response and has potential applications for nanoscale topological optical diodes.

Subsequently, Wang *et al.* studied a similar nonlinear SSH-like circuit, showing how the topological edge state can enhance the harmonic generation.[14] They implemented a significantly longer 1D lattice, with 40 sites, broad operating frequency bands, and clear distinction between the bulk and edge modes. Such a circuit can be viewed as a type of left-handed nonlinear transmission line (NLTL)[196] and supports an SSH-like bandgap with a mid-gap topological boundary state at the fundamental harmonic, as well as propagating-wave modes at higher harmonics. When the circuit was excited at the boundary, cross-phase modulation between the two types of modes gave rise to strongly enhanced generation of third- and higher-harmonic signals, five times higher than in a standard (non-dimerized) NLTL and two orders of magnitude higher than in the lattice's topologically trivial configuration.
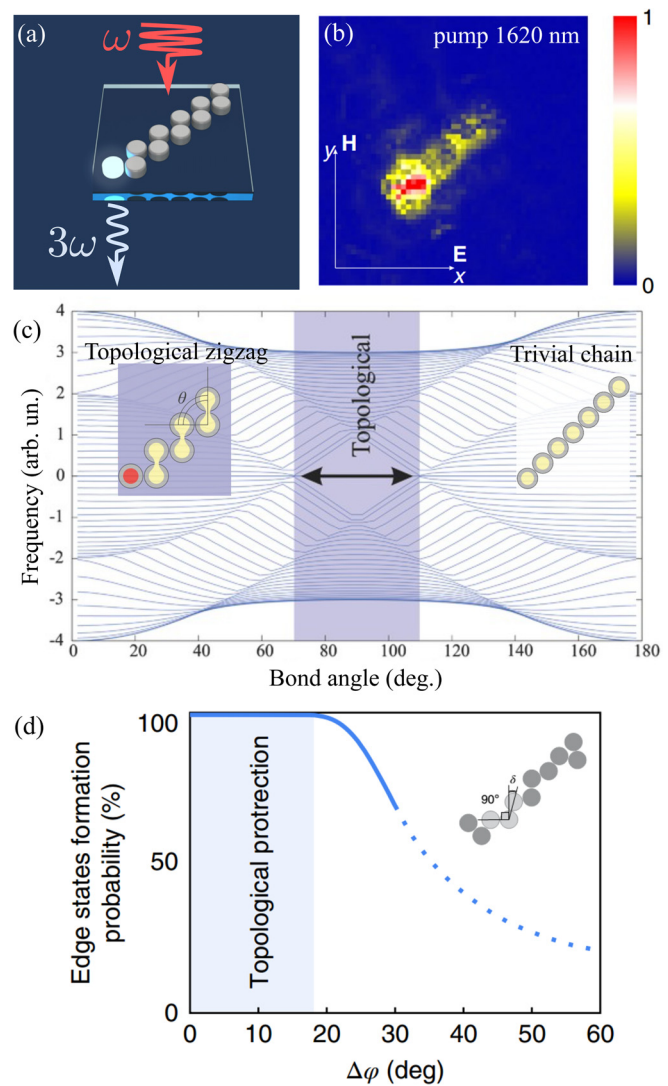

FIG. 11. Nonlinear generation of light from a topological nanostructure.[11] (a) Concept of THG in a zigzag array of nanoresonators: third-harmonic light (frequency 3ω) is generated by the topological edge state. (b) Measured distribution of the third-harmonic field in 11-nanodisk zigzag array of Mie-resonant dielectric nanodisks. (c) Spectrum of the zigzag array calculated as the function of the bond angle. Shaded is the region where the topological edge states can exist.[195] (d) Robustness of the topological state to the disorder: edge state formation persists up to the disorder angle of 20°.

Going to 2D, topology-controlled third harmonic generation was demonstrated in a nanostructured metasurface with a domain wall supporting two counter-propagating spin-polarized edge waves (see Fig. 12). Similar to the earlier theoretical proposal,[37] the topological metasurface was composed of hexamers of silicon nanoparticles. The nontrivial topological properties in the QSHE phase are achieved by deforming a honeycomb lattice of silicon pillars into a triangular lattice of cylinder hexamers, as described in Sec. II.

Figure 12(c) shows the numerically computed bulk band diagram of the structure and the characteristic Dirac-like dispersion of the
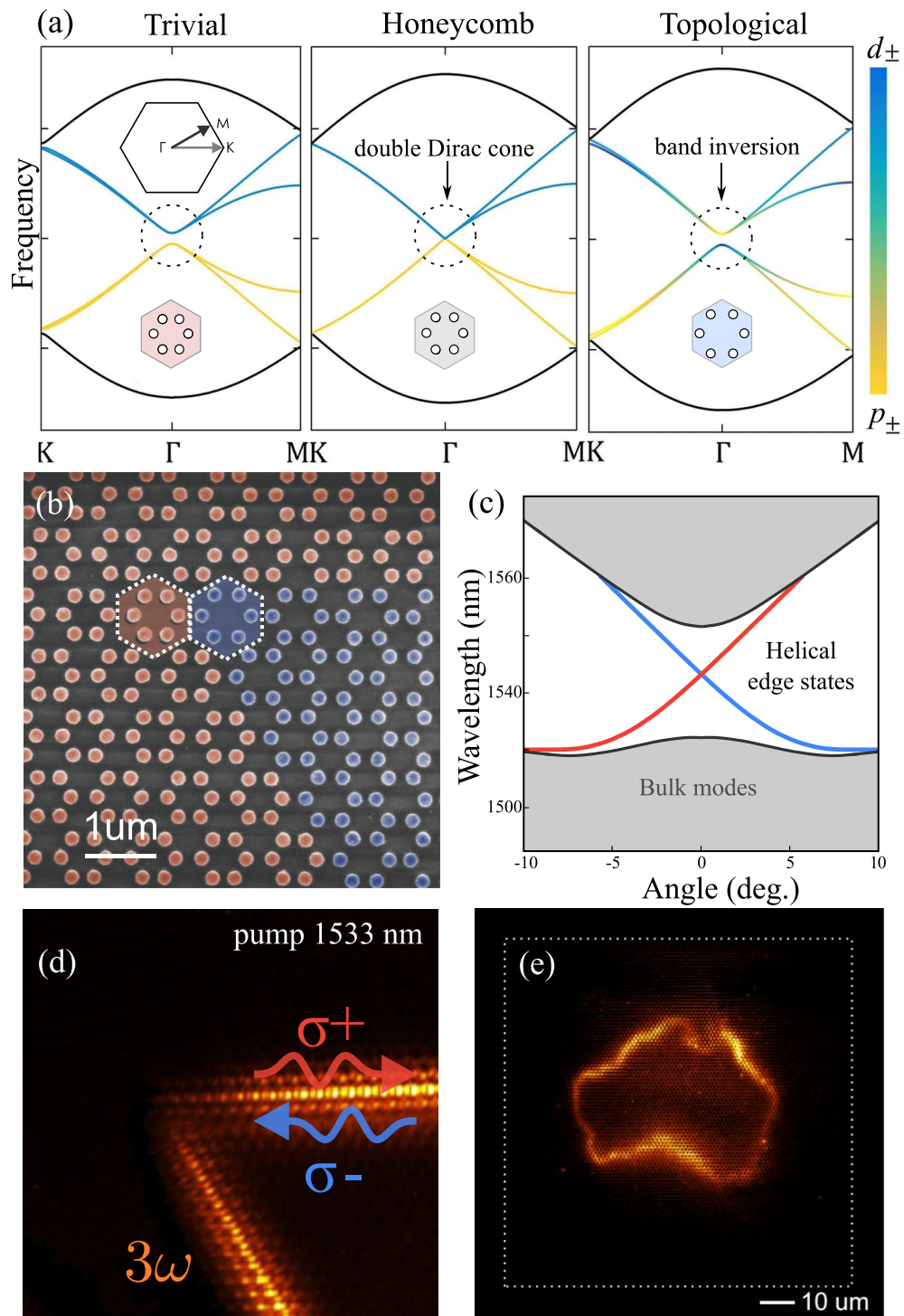
FIG. 12. Third-harmonic generation from nanoscale helical edge states.[69] (a) Topological transition due to clustering the hexagonal unit cell. Band structures for shrunken (left), unperturbed (middle), and expanded (right) lattices of hexamers. Color of the bands encodes polarization ranging from pure circularly polarized dipolar $p_\pm$ to pure circularly polarized quadrupolar $d_\pm$ states. (b) SEM of the fabricated metasurface. (c) Calculated band diagram featuring gapped bands of bulk modes and Dirac-like crossing for the edge states. [(d) and (e)] Experimental images of third-harmonic generation by the edge states at the sharp-corner domain wall (d) and Australia-shaped contour (e). Adapted with permission from Smirnova *et al.*, Phys. Rev. Lett. **123**, 103901 (2019). Copyright 2019 American Physical Society.

spin-momentum locked edge states residing in the bandgap. The two pump polarizations couple to the edge modes with the opposite helicity values σ_+ and σ_-. The metasurface was excited by a tunable pulsed laser, and the third-harmonic signal was imaged onto a camera. The waveguiding domain wall in the geometry-independent photonic topological cavity was then clearly visualized via the third-harmonic field contour, as shown in Fig. 12. Notably, the shorter wavelength of the third harmonic provided the ability to directly image nanoscale helical edge states passing sharp corners with unprecedented resolution.[69]

The above studies all employed topological designs to enhance the localization of the pump beam and hence improve the efficiency of the harmonic generation, without much focus on the modal structure at the harmonic frequency. Very recently, Lan *et al.* have proposed designs for magneto-optical microwave photonic crystals supporting topologically non-trivial bandgaps at both the pump and harmonic wavelengths,[118] enabling traveling wave harmonic generation.

One advantage of traveling wave harmonic generation is that one can design the photonic crystal to have counter-propagating edge states at the fundamental and harmonic frequencies, separating the strong pump from the weak generated signal. Furthermore, the efficiency of the generation can be strongly enhanced by optimizing the edge state dispersion (e.g., via the edge termination) to minimize its group velocity. Conventionally, this slow light-based enhancement is accompanied by an enhanced sensitivity to disorder, which the topological design can overcome. However, for this traveling wave harmonic generation to be efficient it is also necessary to optimize the edge state dispersion to enhance phase matching of the wavevectors to maximize the conversion efficiency.

C. Parametric amplification

In parametric amplification, a small-amplitude signal beam interacts coherently with a strong pump beam. This phase-sensitive interaction can be used to control the topological phase of the signal. For example, a pump beam that breaks time-reversal symmetry explicitly[197] or spontaneously[198] can be used to open topological bandgaps for the small-amplitude signal beam, resulting in chiral edge states which can be used to generate squeezed light.[199]

An alternate approach is to consider parametric amplification in systems that are already topological in the absence of a pump, which is similar in spirit to the harmonic generation discussed above in that both the pump and signal beams propagate in a chiral edge mode. In this case, however, both modes reside typically in the same topological bandgap and therefore, they travel in the same direction. Unidirectional edge states can also offer better phase-matching to maximize frequency conversion. Peano *et al.*[200] studied these processes using a tight-binding model, showing that the frequency conversion is nonreciprocal, and therefore, it suppresses unwanted feedback that limits the performance of such phase-sensitive amplifiers. Later, You *et al.*[201] used rigorous full-wave simulations and coupled-mode theory to demonstrate a strong enhancement of four-wave mixing of topological plasmons in nanopatterned graphene under a strong static magnetic field, predicting a net gain at very low pump powers (10 nW) even in the presence of plasmonic losses.

In addition to the above studies focused on amplification of an external signal beam, parametric amplification of vacuum fluctuations is of special interest for quantum photonic systems; the most common approach for generation of quantum light, being single photons, entangled photon pairs, and correlated biphotons, relies on spontaneous parametric downconversion (SPDC) and spontaneous four-wave mixing (SFWM) in nonlinear media. Thus, nanophotonic structures with modes robust against fabrication disorder and scattering losses can be potentially used to engineer robust, mass-producible quantum light sources and circuits. For example, Ref. 10 has observed reliable and reproducible generation of correlated photon pairs in two-dimensional topological resonator lattices.

Topologically protected biphoton[202] and entangled[203] states were experimentally studied in the SSH-model-based array of coupled silicon nanowaveguides.[204] Biphoton correlation maps resistant against disorder were reported in Refs. 202, using a one-dimensional waveguide array with a single long-long topological defect pumped at an infrared wavelength of 1550 nm. Due to the high third-order nonlinearity of silicon, the photon pairs generated via SFWM overlapped strongly with the topological defect mode localized at one sublattice with the topologically protected propagation constant. Subsequently, strong spatial entanglement between two topological states was revealed in the SSH geometry incorporating two coupled topological defects.[203]

D. Future directions

In addition to potential applications as robust sources of classical and quantum light, the frequency conversion processes also provide the opportunity to implement novel topological lattice models based on synthetic dimensions.[27,28,205] In this approach, the photon energy is treated as a fictitious dimension, along which hopping can be induced by periodic modulation of the refractive index. Recent implementations of this idea have used periodic spatial modulation of waveguide arrays[206] and temporal modulation of resonators,[207,208] but all-optical modulation using nonlinear frequency modulation is also possible. As a promising first step in this direction, Bell *et al.*[209] have demonstrated synthetic one-dimensional lattices with long-range hopping using four wave mixing in a nonlinear optical fiber.

VIII. MANY-BODY QUANTUM EFFECTS
A. Motivation and general approaches

The study of many-body quantum effects in topological photonic systems is motivated both by fundamental interest in emulating novel strongly correlated electronic phases, and also potential practical applications in future quantum computing technologies as a way to robustly store, transport, and manipulate quantum information. Indeed, pursuit of these goals has been a long-standing challenge predating the emergence of topological photonics as its own research field. One is faced with stringent requirements of strong single-photon nonlinearities, comparably strong synthetic gauge fields for light, and minimization of detrimental disorder and losses; combining all these ingredients in topological systems is only now becoming feasible.

The prototypical model for exploring quantum many-body phases is the Bose–Hubbard model, described by the Hamiltonian[210,211]

$$\hat{H}_{\mathrm{BH}} = \sum_{ij} H_{ij} \hat{a}_i^\dagger \hat{a}_j + U \sum_j \hat{a}_j^\dagger \hat{a}_j^\dagger \hat{a}_j \hat{a}_j, \qquad (14)$$

where H_{ij} describes linear on-site energies and inter-site couplings [cf. Eq. (1)] and U is the photon-photon interaction strength. In the mean

field limit, Eq. (14) reduces to the nonlinear Schrödinger equation similar to the ones discussed in Sec. V. Since strong single photon interactions are quite difficult to realize, several recent studies have explored the emulation of one-dimensional two-particle quantum dynamics using specially designed two-dimensional classical lattices.[212–216]

In the case of a simple 1D lattice, Eq. (14) exhibits a transition from a superfluid phase to a Mott insulator phase as the interaction strength is increased.[211] Driven-dissipative extensions of the Bose–Hubbard model are often required to account for inevitable photon losses.[100] The interplay between photon-photon interactions, dissipation, pumping, disorder, and the lattice geometry and topology gives rise to rich behavior qualitatively different from the classical limit.[217–222] For example, topological adiabatic pumping, which can break down in nonlinear systems due to instabilities, can become robust again in the presence of strong single photon interactions.[223,224] For further background on this extensive topic, we refer the reader to earlier review articles,[3,210,211] and in the following focus on the most recent developments.

B. Strong interactions in synthetic magnetic fields

Combining strong single photon interactions with synthetic magnetic fields is of tremendous interest as a means of creating photonic analogs of fractional QH states.[225–227] Efforts in this direction have focused on two platforms: superconducting circuits[121,122] and Rydberg atoms.[98,115,116]

One can create synthetic gauge fields for superconducting resonator arrays by periodically modulating in time either their resonant frequencies, or the inter-resonator hopping strength.[220,223] The latter approach was demonstrated by Roushan et al. in 2017 in the simplest possible system supporting a nonzero synthetic magnetic flux, a triangular three cavity array.[121] Under the synthetic magnetic flux, a single photon injected into one site exhibited chiral dynamics. Due to the strong interactions, two photon states circulated in the opposite direction. This approach, when scaled up to larger arrays, is expected to yield photonic fractional QH states.

Related experiments by the same group have probed the 1D Harper–Hofstadter model in the strong interaction regime.[122] The Harper–Hofstadter model emulates a 2D tight binding lattice under a uniform magnetic field, exhibiting the characteristic Hofstadter butterfly eigenvalue spectrum as the effective magnetic field strength is tuned. Due to the purely 1D geometry of this system, a larger number of sites (9) were accessible, and time-domain spectroscopy was used to measure both the single photon spectrum and signatures of many body localization in the two photon spectrum.

Successful realization of a photonic fractional QH state, the Laughlin state, was recently demonstrated by Clark et al. using ultracold Rydberg atoms in a twisted cavity.[115] The twisted cavity created an effective magnetic field for light, with Floquet modulation used to compensate for imperfections in the cavity and achieve a highly degenerate Landau level spectrum.[98] The strong single photon nonlinearity enabled by the Rydberg atoms induced two-photon scattering between different degenerate orbital angular momentum modes in the Landau level. Measuring the spatial structure of the optical field after injecting two photons into the cavity, a circularly symmetric annular intensity profile and angle-dependent two-photon correlations were observed as key signatures of the Laughlin state, shown in Fig. 13.
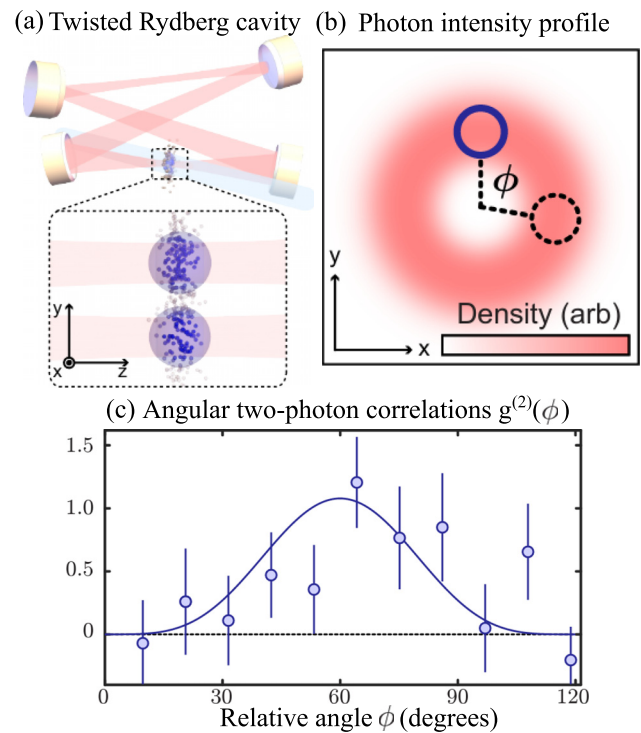

(a) Twisted Rydberg cavity   (b) Photon intensity profile

(c) Angular two-photon correlations $g^{(2)}(\phi)$

FIG. 13. Observation of a photonic Laughlin state.[115] (a) Twisted cavity with nonlinear interactions mediated by Rydberg atoms. (b) Circularly symmetric photon intensity profile. (c) Measured two photon correlations are not circularly symmetric, but depend on the relative angular position of the two photons. A solid curve indicates the expected correlations of the Laughlin state, with minima at integer multiples of $120°$. Adapted with permission from Clark et al., arXiv:1907.05872 (2019). Copyright 2019 Author.

C. Future directions

To generate photonic fractional QH states using superconducting circuit arrays, the approach of Roushan et al. will have to be scaled up to larger two-dimensional arrays.[121] Two-dimensional arrays are more challenging to fabricate, not only due to the larger number of sites, but also because it is more difficult to integrate the required control circuitry while keeping inevitable decoherence effects to an acceptable level. Nevertheless, due to the tremendous interest in quantum computing using superconducting arrays, particularly the use of fractional QH states as anyons for topological quantum computation, these issues will likely be overcome in the near future.

Most experimental efforts (both in the non-interacting and strongly interacting regimes) have focused on the generation and transport of two-photon quantum states, requiring small system sizes to ensure appreciable interaction effects. To reach the full many-body regime, it will be necessary to scale up these experiments to larger lattices while maintaining an appreciable photon number density. Theoretical predictions for novel topological phenomena emerging for several interacting photons will provide useful stepping stones for achieving this goal. Conversely, with recent demonstrations of strongly interacting two photon states using Rydberg atoms and superconducting circuits, there are now many interesting theoretical predictions to test.[3,213,216,223]

IX. CONCLUSIONS AND OUTLOOK

We have reviewed the basic physics and practical implementations of photonic systems that combine the studies of topological phases with nonlinear optics. Such systems can be modeled by nonlinear tight-binding models or nonlinear continuous-wave equations. Currently, there is a plethora of theoretical predictions of nonlinear phenomena in topological photonic structures, including solitons, modulational instability, frequency conversion, and optical switching. Many of these are now starting to be realized in experiments: the past two years have seen the first experimental demonstrations of lasing,[8,53,160–162] harmonic generation,[11,14,228] nonlinearly induced topological edge states,[101] bulk solitons emerging from topological bands,[148] and Laughlin states of light.[115]

Topological dielectric nanostructures are another highly promising platform for future experimental studies. Topological nanostructures can be used to create robust components such as unidirectional waveguides,[66] miniature topological cavities,[190] low-power nanoscale lasers,[94] and nonlinear light sources,[69] whose properties can be tuned via topological phase transitions. Connections with the older field of singular optics are now starting to be appreciated, e.g., in the polarization-controlled propagation direction of QSH edge states.

In nonlinear circuits, there are numerous opportunities to study further topological phenomena. For instance, not all of the predicted properties of topological solitons have been definitively observed in circuit experiments, such as the frequency detuning and non-exponential decay profiles of 1D solitons.[144] It is presently unclear whether or to what extent the sublattice trick, which proved useful for simulating T-breaking in linear circuits, can co-exist with nonlinear circuit elements.[71,124] Achieving real or effective T-breaking in a 2D electronic circuit would enable intriguing applications such as robust traveling wave amplification.[200] It would also be interesting to explore how nonlinearities affect topological phenomena that rely intrinsically on non-Hermiticity, which have already been studied in linear circuits with resistive elements.[125]

For many practical applications, reconfigurability and dynamic tunability of photonic topological insulators are essential. In Ref. 158, the position of the topological bandgap in a pillar photonic crystal was proposed to be tuned by modifying the refractive index of a liquid crystal background medium with external electric field. Later, optical control over the spectral position of edge states was implemented using pump-induced carrier generation in a topological photonic crystal slab.[229] Two theoretical proposals were made by Shalaev's group for ring resonators to realize switchable topological phase transitions, based on thermal tuning[230] and integration with transparent conducting oxides.[231] The development of electrically or optically tunable photonic topological insulators is another important direction for future research.

While the study of electronic topological states has a long history, topological photonics is a comparatively young field of research. A pressing question now is how to harness this newly discovered degree of freedom in optical devices, for example, to design and fabricate disorder-immune components for high-speed information transfer and processing. As with conventional optical components, understanding and exploiting nonlinear effects offers many new opportunities, such as:

- Nonlinearities provide a straightforward way to reconfigure or otherwise manipulate topological lattices, and they are particularly essential for achieving ultra-fast modulation.[12]

- Parametric frequency conversion processes are technologically important. Feedback suppression enabled by certain topological edge states may be useful for stabilizing traveling wave amplifiers.[199,200] Spontaneous wave mixing processes are an important source of entangled photon pairs for integrated quantum photonics applications.

- Lasers are ubiquitous, and they become inherently nonlinear devices above threshold due to gain saturation, as well as they are always non-Hermitian. Topological edge states may be useful for the mode stabilization enabling high-power single-mode operation, although the extent to which this stabilization may hold in realistic devices is still under debate.

- At a more fundamental level, nonlinear topological photonics provides a playground for exploring novel nonlinear wave equations originally derived in the context of high energy physics and potentially realizing them in tabletop experiments. These models can support novel mechanisms for soliton formation (e.g., topological solitons and embedded solitons).

We envision nonlinear topological photonics to provide a fertile playground for not only studying interesting theoretical problems at the borderland between nonlinear dynamics and topology, but also as a route toward novel designs for disorder-robust photonic device applications, such as high-speed routing and switching, nanoscale lasers, and quantum light sources.

ACKNOWLEDGMENTS

REFERENCES

[1] M. Z. Hasan and C. L. Kane, "Colloquium: Topological insulators," Rev. Mod. Phys. **82**, 3045–3067 (2010).

[2] L. Lu, J. D. Joannopoulos, and M. Soljačić, "Topological states in photonic systems," Nat. Phys. **12**, 626–629 (2016).

[3] T. Ozawa, H. M. Price, A. Amo, N. Goldman, M. Hafezi, L. Lu, M. C. Rechtsman, D. Schuster, J. Simon, O. Zilberberg, and I. Carusotto, "Topological photonics," Rev. Mod. Phys. **91**, 015006 (2019).

[4] B.-Y. Xie, H.-F. Wang, X.-Y. Zhu, M.-H. Lu, Z. D. Wang, and Y.-F. Chen, "Photonics meets topology," Opt. Express **26**, 24531 (2018).

[5] S. Longhi, "Parity-time symmetry meets photonics: A new twist in non-Hermitian optics," Europhys. Lett. **120**, 64001 (2017).

[6] X. Zhou, Y. Wang, D. Leykam, and Y. D. Chong, "Optical isolation with nonlinear topological photonics," New J. Phys. **19**, 095002 (2017).

[7] Y. V. Kartashov and D. V. Skryabin, "Bistable topological insulator with exciton-polaritons," Phys. Rev. Lett. **119**, 253904 (2017).

[8] M. A. Bandres, S. Wittek, G. Harari, M. Parto, J. Ren, M. Segev, D. N. Christodoulides, and M. Khajavikhan, "Topological insulator laser: Experiments," Science **359**, eaar4005 (2018).

[9] W. Chen, D. Leykam, Y. Chong, and L. Yang, "Nonreciprocity in synthetic photonic materials with nonlinearity," MRS Bull. **43**, 443–451 (2018).

[10] S. Mittal, E. A. Goldschmidt, and M. Hafezi, "A topological source of quantum light," Nature **561**, 502–506 (2018).

[11] S. Kruk, A. Poddubny, D. Smirnova, L. Wang, A. Slobozhanyuk, A. Shorokhov, I. Kravchenko, B. Luther-Davies, and Y. Kivshar, "Nonlinear light generation in topological nanostructures," Nat. Nanotechnol. **14**, 126–130 (2019).

[12]D. Leykam, S. Mittal, M. Hafezi, and Y. D. Chong, "Reconfigurable topological phases in next-nearest-neighbor coupled resonator lattices," Phys. Rev. Lett. **121**, 023901 (2018).

[13]A. Amo, "When quantum optics meets topology," Science **359**, 638–639 (2018).

[14]Y. Wang, L.-J. Lang, C. H. Lee, B. Zhang, and Y. D. Chong, "Topologically enhanced harmonic generation in a nonlinear transmission line metamaterial," Nat. Commun. **10**, 1102 (2019).

[15]S. Barik and M. Hafezi, "Robust and compact waveguides," Nat. Nanotechnol. **14**, 8–9 (2019).

[16]M. I. Shalaev, W. Walasik, A. Tsukernik, Y. Xu, and N. M. Litchinitser, "Robust topologically protected transport in photonic crystals at telecommunication wavelengths," Nat. Nanotechnol. **14**, 31–34 (2019).

[17]C. Husko, A. De Rossi, S. Combrié, Q. V. Tran, F. Raineri, and C. W. Wong, "Ultrafast all-optical modulation in GaAs photonic crystal cavities," Appl. Phys. Lett. **94**, 021111 (2009).

[18]B. Eggleton, T. Vo, R. Pant, J. Schr, M. Pelusi, D. Y. Choi, S. Madden, and B. Luther-Davies, "Photonic chip based ultrafast optical processing based on high nonlinearity dispersion engineered chalcogenide waveguides," Laser Photonics Rev. **6**, 97–114 (2012).

[19]K. Y. Bliokh, D. Smirnova, and F. Nori, "Quantum spin Hall effect of light," Science **348**, 1448–1451 (2015).

[20]M. G. Silveirinha, "Bulk-edge correspondence for topological photonic continua," Phys. Rev. B **94**, 205105 (2016).

[21]K. Y. Bliokh, D. Leykam, M. Lein, and F. Nori, "Topological non-Hermitian origin of surface Maxwell waves," Nat. Commun. **10**, 580 (2019).

[22]T. Van Mechelen and Z. Jacobi, "Unidirectional Maxwellian spin waves," Nanophotonics **8**, 1399 (2019).

[23]D. Hsieh, J. W. McIver, D. H. Torchinsky, D. R. Gardner, Y. S. Lee, and N. Gedik, "Nonlinear optical probe of tunable surface electrons on a topological insulator," Phys. Rev. Lett. **106**, 057401 (2011).

[24]C. Zhao, H. Zhang, X. Qi, Y. Chen, Z. Wang, S. Wen, and D. Tang, "Ultra-short pulse generation by a topological insulator based saturable absorber," Appl. Phys. Lett. **101**, 211106 (2012).

[25]S. Chen, C. Zhao, Y. Li, H. Huang, S. Lu, H. Zhang, and S. Wen, "Broadband optical and microwave nonlinear response in topological insulator," Opt. Mater. Express **4**, 587–596 (2014).

[26]H. C. Manoharan, "A romance with many dimensions," Nat. Nanotechnol. **5**, 477–479 (2010).

[27]T. Ozawa, H. M. Price, N. Goldman, O. Zilberberg, and I. Carusotto, "Synthetic dimensions in integrated photonics: From optical isolation to four-dimensional quantum Hall physics," Phys. Rev. A **93**, 043827 (2016).

[28]L. Yuan, Q. Lin, M. Xiao, and S. Fan, "Synthetic dimension in photonics," Optica **5**, 1396–1405 (2018).

[29]K. von Klitzing, "The quantized Hall effect," Rev. Mod. Phys. **58**, 519–531 (1986).

[30]D. J. Thouless, M. Kohmoto, M. P. Nightingale, and M. den Nijs, "Quantized Hall conductance in a two-dimensional periodic potential," Phys. Rev. Lett. **49**, 405–408 (1982).

[31]C. L. Kane and E. J. Mele, "Z_2 topological order and the quantum spin Hall effect," Phys. Rev. Lett. **95**, 146802 (2005).

[32]B. A. Bernevig, T. L. Hughes, and S.-C. Zhang, "Quantum spin Hall effect and topological phase transition in HgTe quantum wells," Science **314**, 1757–1761 (2006).

[33]M. König, S. Wiedmann, C. Brüne, A. Roth, H. Buhmann, L. W. Molenkamp, X.-L. Qi, and S.-C. Zhang, "Quantum spin Hall insulator state in HgTe quantum wells," Science **318**, 766–770 (2007).

[34]B. A. Volkov and O. A. Pankratov, "Two-dimensional massless electrons in an inverted contact," JETP Lett. **42**, 178 (1985).

[35]L. G. Gerchikov and A. V. Subashiev, "Interface states in subband structure of semiconductor quantum wells," Phys. Status Solidi B **160**, 443–457 (1990).

[36]B. Bernevig and T. Hughes, *Topological Insulators and Topological Superconductors* (Princeton University Press, 2013).

[37]L.-H. Wu and X. Hu, "Scheme for achieving a topological photonic crystal by using dielectric material," Phys. Rev. Lett. **114**, 223901 (2015).

[38]G. W. Semenoff, V. Semenoff, and F. Zhou, "Domain walls in gapped graphene," Phys. Rev. Lett. **101**, 087204 (2008).

[39]W. Yao, S. A. Yang, and Q. Niu, "Edge states in graphene: From gapped flat-band to gapless chiral modes," Phys. Rev. Lett. **102**, 096801 (2009).

[40]T. Kitagawa, E. Berg, M. Rudner, and E. Demler, "Topological characterization of periodically driven quantum systems," Phys. Rev. B **82**, 235114 (2010).

[41]N. H. Lindner, G. Refael, and V. Galitski, "Floquet topological insulator in semiconductor quantum wells," Nat. Phys. **7**, 490–495 (2011).

[42]M. S. Rudner, N. H. Lindner, E. Berg, and M. Levin, "Anomalous edge states and the bulk-edge correspondence for periodically driven two-dimensional systems," Phys. Rev. X **3**, 031005 (2013).

[43]Y. E. Kraus, Y. Lahini, Z. Ringel, M. Verbin, and O. Zilberberg, "Topological states and adiabatic pumping in quasicrystals," Phys. Rev. Lett. **109**, 106402 (2012).

[44]W. A. Benalcazar, B. A. Bernevig, and T. L. Hughes, "Quantized electric multipole insulators," Science **357**, 61–66 (2017).

[45]L. Lu, J. D. Joannopoulos, and M. Soljačić, "Topological photonics," Nat. Photonics **8**, 821–829 (2014).

[46]A. B. Khanikaev and G. Shvets, "Two-dimensional topological photonics," Nat. Photonics **11**, 763–773 (2017).

[47]X.-C. Sun, C. He, X.-P. Liu, M.-H. Lu, S.-N. Zhu, and Y.-F. Chen, "Two-dimensional topological photonic systems," Prog. Quantum Electron. **55**, 52–73 (2017).

[48]M. S. Rider, S. J. Palmer, S. R. Pocock, X. Xiao, P. A. Huidobro, and V. Giannini, "A perspective on topological nanophotonics: Current status and future challenges," J. Appl. Phys. **125**, 120901 (2019).

[49]S.-Q. Shen, *Topological Insulators. Dirac Equation in Condensed Matters*, Springer Series in Solid-State Sciences (Springer, Heidelberg, 2013).

[50]Z. Wang, Y. Chong, J. D. Joannopoulos, and M. Soljačić, "Observation of unidirectional backscattering-immune topological electromagnetic states," Nature **461**, 772–775 (2009).

[51]M. C. Rechtsman, J. M. Zeuner, Y. Plotnik, Y. Lumer, D. Podolsky, F. Dreisow, S. Nolte, M. Segev, and A. Szameit, "Photonic Floquet topological insulators," Nature **496**, 196 (2013).

[52]A. Slobozhanyuk, A. V. Shchelokova, X. Ni, S. Hossein Mousavi, D. A. Smirnova, P. A. Belov, A. Alú, Y. S. Kivshar, and A. B. Khanikaev, "Near-field imaging of spin-locked edge states in all-dielectric topological metasurfaces," Appl. Phys. Lett. **114**, 031103 (2019).

[53]B. Bahari, A. Ndao, F. Vallini, A. El Amili, Y. Fainman, and B. Kanté, "Nonreciprocal lasing in topological cavities of arbitrary geometries," Science **358**, 636–640 (2017).

[54]F. D. M. Haldane and S. Raghu, "Possible realization of directional optical waveguides in photonic crystals with broken time-reversal symmetry," Phys. Rev. Lett. **100**, 013904 (2008).

[55]S. Raghu and F. D. M. Haldane, "Analogs of quantum-Hall-effect edge states in photonic crystals," Phys. Rev. A **78**, 033834 (2008).

[56]Z. Wang, Y. D. Chong, J. D. Joannopoulos, and M. Soljačić, "Reflection-free one-way edge modes in a gyromagnetic photonic crystal," Phys. Rev. Lett. **100**, 013905 (2008).

[57]M. Verbin, O. Zilberberg, Y. E. Kraus, Y. Lahini, and Y. Silberberg, "Observation of topological phase transitions in photonic quasicrystals," Phys. Rev. Lett. **110**, 076403 (2013).

[58]M. Hafezi, S. Mittal, J. Fan, A. Migdall, and J. M. Taylor, "Imaging topological edge states in silicon photonics," Nat. Photonics **7**, 1001 (2013).

[59]A. Slobozhanyuk, S. H. Mousavi, X. Ni, D. Smirnova, Y. S. Kivshar, and A. B. Khanikaev, "Three-dimensional all-dielectric photonic topological insulator," Nat. Photonics **11**, 130–136 (2017).

[60]M. Hafezi, E. A. Demler, M. D. Lukin, and J. M. Taylor, "Robust optical delay lines with topological protection," Nat. Phys. **7**, 907–912 (2011).

[61]A. B. Khanikaev, S. Hossein Mousavi, W.-K. Tse, M. Kargarian, A. H. MacDonald, and G. Shvets, "Photonic topological insulators," Nat. Mater. **12**, 233–239 (2013).

[62]T. Ma, A. B. Khanikaev, S. H. Mousavi, and G. Shvets, "Guiding electromagnetic waves around sharp corners: Topologically protected photonic transport in metawaveguides," Phys. Rev. Lett. **114**, 127401 (2015).

[63]A. P. Slobozhanyuk, A. B. Khanikaev, D. S. Filonov, D. A. Smirnova, A. E. Miroshnichenko, and Y. S. Kivshar, "Experimental demonstration of topological effects in bianisotropic metamaterials," Sci. Rep. **6**, 22270 (2016).

[64]T. Ma and G. Shvets, "All-Si valley-Hall photonic topological insulator," New J. Phys. **18**, 025012 (2016).

[65]M. A. Gorlach, X. Ni, D. A. Smirnova, D. Korobkin, D. Zhirihin, A. P. Slobozhanyuk, P. A. Belov, A. Alù, and A. B. Khanikaev, "Far-field probing of leaky topological states in all-dielectric metasurfaces," Nat. Commun. **9**, 909 (2018).

[66]S. Barik, A. Karasahin, C. Flower, T. Cai, H. Miyake, W. DeGottardi, M. Hafezi, and E. Waks, "A topological quantum optics interface," Science **359**, 666 (2018).

[67]X.-T. He, E.-T. Liang, J.-J. Yuan, H.-Y. Qiu, X.-D. Chen, F.-L. Zhao, and J.-W. Dong, "A silicon-on-insulator slab for topological valley transport," Nat. Commun. **10**, 872 (2019).

[68]S. Peng, N. J. Schilder, X. Ni, J. van de Groep, M. L. Brongersma, A. Alù, A. B. Khanikaev, H. A. Atwater, and A. Polman, "Probing the band structure of topological silicon photonic lattices in the visible spectrum," Phys. Rev. Lett. **122**, 117401 (2019).

[69]D. Smirnova, S. Kruk, D. Leykam, E. Melik-Gaykazyan, D.-Y. Choi, and Y. Kivshar, "Third-harmonic generation in photonic topological metasurfaces," Phys. Rev. Lett. **123**, 103901 (2019).

[70]J. Noh, S. Huang, K. P. Chen, and M. C. Rechtsman, "Observation of photonic topological valley Hall edge states," Phys. Rev. Lett. **120**, 063902 (2018).

[71]J. Ningyuan, C. Owens, A. Sommer, D. Schuster, and J. Simon, "Time- and site-resolved dynamics in a topological circuit," Phys. Rev. X **5**, 021031 (2015).

[72]Y. Li, Y. Sun, W. Zhu, Z. Guo, J. Jiang, T. Kariyado, H. Chen, and X. Hu, "Topological LC-circuits based on microstrips and observation of electromagnetic modes with orbital angular momentum," Nat. Commun. **9**, 4598 (2018).

[73]M. V. Berry, "Quantal phase factors accompanying adiabatic changes," Proc. R. Soc., A **392**, 45–57 (1984).

[74]D. Leykam and A. S. Desyatnikov, "Conical intersections for light and matter waves," Adv. Phys.: X **1**, 101–113 (2016).

[75]J. Zak, "Berry's phase for energy bands in solids," Phys. Rev. Lett. **62**, 2747–2750 (1989).

[76]O. Peleg, G. Bartal, B. Freedman, O. Manela, M. Segev, and D. N. Christodoulides, "Conical diffraction and gap solitons in honeycomb photonic lattices," Phys. Rev. Lett. **98**, 103901 (2007).

[77]S. Bittner, B. Dietz, M. Miski-Oglu, P. Oria Iriarte, A. Richter, and F. Schäfer, "Observation of a Dirac point in microwave experiments with a photonic crystal modeling graphene," Phys. Rev. B **82**, 014301 (2010).

[78]M. Bellec, U. Kuhl, G. Montambaux, and F. Mortessagne, "Topological transition of Dirac points in a microwave experiment," Phys. Rev. Lett. **110**, 033902 (2013).

[79]M. Bellec, U. Kuhl, G. Montambaux, and F. Mortessagne, "Manipulation of edge states in microwave artificial graphene," New J. Phys. **16**, 113023 (2014).

[80]T. Jacqmin, I. Carusotto, I. Sagnes, M. Abbarchi, D. D. Solnyshkov, G. Malpuech, E. Galopin, A. Lemaître, J. Bloch, and A. Amo, "Direct observation of Dirac cones and a flatband in a honeycomb lattice for polaritons," Phys. Rev. Lett. **112**, 116402 (2014).

[81]D. Song, V. Paltoglou, S. Liu, Y. Zhu, D. Gallardo, L. Tang, J. Xu, M. Ablowitz, N. K. Efremidis, and Z. Chen, "Unveiling pseudospin and angular momentum in photonic graphene," Nat. Commun. **6**, 6272 (2015).

[82]Z. Zhang, F. Li, G. Malpuech, Y. Zhang, O. Bleu, S. Koniakhin, C. Li, Y. Zhang, M. Xiao, and D. D. Solnyshkov, "Particlelike behavior of topological defects in linear wave packets in photonic graphene," Phys. Rev. Lett. **122**, 233905 (2019).

[83]R. Guo, M. Nečada, T. K. Hakala, A. I. Väkeväinen, and P. Törmä, "Lasing at K points of a honeycomb plasmonic lattice," Phys. Rev. Lett. **122**, 013901 (2019).

[84]F. D. M. Haldane, "Model for a quantum Hall effect without Landau levels: Condensed-matter realization of the 'parity anomaly,'" Phys. Rev. Lett. **61**, 2015–2018 (1988).

[85]S. A. Dyakov, A. Baldycheva, T. S. Perova, G. V. Li, E. V. Astrova, N. A. Gippius, and S. G. Tikhodeev, "Surface states in the optical spectra of two-dimensional photonic crystals with various surface terminations," Phys. Rev. B **86**, 115126 (2012).

[86]Y. S. Kivshar, "Nonlinear Tamm states and surface effects in periodic photonic structures," Laser Phys. Lett. **5**, 703–713 (2008).

[87]H. S. Eisenberg, Y. Silberberg, R. Morandotti, A. R. Boyd, and J. S. Aitchison, "Discrete spatial optical solitons in waveguide arrays," Phys. Rev. Lett. **81**, 3383–3386 (1998).

[88]A. Szameit, D. Blömer, J. Burghoff, T. Schreiber, T. Pertsch, S. Nolte, A. Tünnermann, and F. Lederer, "Discrete nonlinear localization in femtosecond laser written waveguides in fused silica," Opt. Express **13**, 10552–10557 (2005).

[89]J. W. Fleischer, T. Carmon, M. Segev, N. K. Efremidis, and D. N. Christodoulides, "Observation of discrete solitons in optically induced real time waveguide arrays," Phys. Rev. Lett. **90**, 023902 (2003).

[90]R. Iwanow, R. Schiek, G. I. Stegeman, T. Pertsch, F. Lederer, Y. Min, and W. Sohler, "Observation of discrete quadratic solitons," Phys. Rev. Lett. **93**, 113902 (2004).

[91]M. Li, S. Huang, Q. Wang, H. Petek, and K. P. Chen, "Nonlinear optical localization in embedded chalcogenide waveguide arrays," AIP Adv. **4**, 057120 (2014).

[92]L. Fan, J. Wang, L. T. Varghese, H. Shen, B. Niu, Y. Xuan, A. M. Weiner, and M. Qi, "An all-silicon passive optical diode," Science **335**, 447–450 (2012).

[93]Y. Yu, Y. Chen, H. Hu, W. Xue, K. Yvind, and J. Mork, "Nonreciprocal transmission in a nonlinear photonic-crystal Fano structure with broken symmetry," Laser Photonics Rev. **9**, 241–247 (2015).

[94]Y. Ota, R. Katsumi, K. Watanabe, S. Iwamoto, and Y. Arakawa, "Topological photonic crystal nanocavity laser," Commun. Phys. **1**, 86 (2018).

[95]M. Wimmer, A. Regensburger, M.-A. Miri, C. Bersch, D. N. Christodoulides, and U. Peschel, "Observation of optical solitons in PT-symmetric lattices," Nat. Commun. **6**, 7782 (2015).

[96]D. Tanese, H. Flayac, D. Solnyshkov, A. Amo, A. Lemaître, E. Galopin, R. Braive, P. Senellart, I. Sagnes, G. Malpuech, and J. Bloch, "Polariton condensation in solitonic gap states in a one-dimensional periodic potential," Nat. Commun. **4**, 1749 (2013).

[97]Z. Zhang, R. Wang, Y. Zhang, Y. V. Kartashov, F. Li, H. Zhong, H. Guan, K. Gao, F. Li, Y. Zhang, and M. Xiao, "Observation of edge solitons in photonic graphene," Nat. Commun. **11**, 1902 (2020).

[98]L. W. Clark, N. Jia, N. Schine, C. Baum, A. Georgakopoulos, and J. Simon, "Interacting Floquet polaritons," Nature **571**, 532–536 (2019).

[99]D. A. Dobrykh, A. V. Yulin, A. P. Slobozhanyuk, A. N. Poddubny, and Y. S. Kivshar, "Nonlinear control of electromagnetic topological edge states," Phys. Rev. Lett. **121**, 163901 (2018).

[100]R. Ma, B. Saxberg, C. Owens, N. Leung, Y. Lu, J. Simon, and D. I. Schuster, "A dissipatively stabilized Mott insulator of photons," Nature **566**, 51–57 (2019).

[101]Y. Hadad, J. C. Soric, A. B. Khanikaev, and A. Alù, "Self-induced topological protection in nonlinear circuit arrays," Nat. Electron. **1**, 178–182 (2018).

[102]D. N. Christodoulides and R. I. Joseph, "Discrete self-focusing in nonlinear arrays of coupled waveguides," Opt. Lett. **13**, 794–796 (1988).

[103]F. Lederer, G. I. Stegeman, D. N. Christodoulides, G. Assanto, M. Segev, and Y. Silberberg, "Discrete solitons in optics," Phys. Rep. **463**, 1–126 (2008).

[104]C. Denz, S. Flach, Y. S. Kivshar et al., Nonlinearities in Periodic Structures and Metamaterials (Springer, 2010), Vol. 150.

[105]Z. Chen, M. Segev, and D. N. Christodoulides, "Optical spatial solitons: Historical overview and recent advances," Rep. Prog. Phys. **75**, 086401 (2012).

[106]Y. Lahini, E. Frumker, Y. Silberberg, S. Droulias, K. Hizanidis, R. Morandotti, and D. N. Christodoulides, "Discrete X-wave formation in nonlinear waveguide arrays," Phys. Rev. Lett. **98**, 023901 (2007).

[107]A. Bisianov, M. Wimmer, U. Peschel, and O. A. Egorov, "Stability of topologically protected edge states in nonlinear fiber loops," Phys. Rev. A **100**, 063830 (2019).

[108]C. Schneider, K. Winkler, M. D. Fraser, M. Kamp, Y. Yamamoto, E. A. Ostrovskaya, and S. Höfling, "Exciton-polariton trapping and potential landscape engineering," Rep. Prog. Phys. **80**, 016503 (2017).

[109]A. I. Kuznetsov, A. E. Miroshnichenko, M. L. Brongersma, Y. S. Kivshar, and B. Luk'yanchuk, "Optically resonant dielectric nanostructures," Science **354**, aag2472 (2016).

[110]D. Smirnova and Y. S. Kivshar, "Multipolar nonlinear nanophotonics," Optica **3**, 1241 (2016).

[111]M. R. Shcherbakov, D. N. Neshev, B. Hopkins, A. S. Shorokhov, I. Staude, E. V. Melik-Gaykazyan, M. Decker, A. A. Ezhov, A. E. Miroshnichenko, I. Brener, A. A. Fedyanin, and Y. S. Kivshar, "Enhanced third-harmonic generation in silicon nanoparticles driven by magnetic response," Nano Lett. **14**, 6488–6492 (2014).

[112] D. A. Smirnova, A. B. Khanikaev, L. A. Smirnov, and Y. S. Kivshar, "Multipolar third-harmonic generation driven by optically induced magnetic resonances," ACS Photonics **3**, 1468 (2016).

[113] R. Camacho-Morales, M. Rahmani, S. Kruk, L. Wang, L. Xu, D. A. Smirnova, A. S. Solntsev, A. Miroshnichenko, H. H. Tan, F. Karouta, S. Naureen, K. Vora, L. Carletti, C. D. Angelis, C. Jagadish, Y. S. Kivshar, and D. N. Neshev, "Nonlinear generation of vector beams from AlGaAs nanoantennas," Nano Lett. **16**, 7191–7197 (2016).

[114] K. Frizyuk, I. Volkovskaya, D. Smirnova, A. Poddubny, and M. Petrov, "Second-harmonic generation in Mie-resonant dielectric nanoparticles made of noncentrosymmetric materials," Phys. Rev. B **99**, 075425 (2019).

[115] L. W. Clark, N. Schine, C. Baum, N. Jia, and J. Simon, "Observation of Laughlin states made of light," arXiv:1907.05872 (2019).

[116] S. de Léséleuc, V. Lienhard, P. Scholl, D. Barredo, S. Weber, N. Lang, H. P. Büchler, T. Lahaye, and A. Browaeys, "Observation of a symmetry-protected topological phase of interacting bosons with Rydberg atoms," Science **365**, 775–780 (2019).

[117] Z. Zhang, Y. Zhang, J. Sheng, L. Yang, M.-A. Miri, D. N. Christodoulides, B. He, Y. Zhang, and M. Xiao, "Observation of parity-time symmetry in optically induced atomic lattices," Phys. Rev. Lett. **117**, 123601 (2016).

[118] Z. Lan, J. W. You, and N. C. Panoiu, "Nonlinear one-way edge-mode interactions for frequency mixing in topological photonic crystals," Phys. Rev. B **101**, 155422 (2020).

[119] B. M. Anderson, R. Ma, C. Owens, D. I. Schuster, and J. Simon, "Engineering topological many-body materials in microwave cavity arrays," Phys. Rev. X **6**, 041043 (2016).

[120] C. Owens, A. LaChapelle, B. Saxberg, B. M. Anderson, R. Ma, J. Simon, and D. I. Schuster, "Quarter-flux Hofstadter lattice in a qubit-compatible microwave cavity array," Phys. Rev. A **97**, 013818 (2018).

[121] P. Roushan, C. Neill, A. Megrant, Y. Chen, R. Babbush, R. Barends, B. Campbell, Z. Chen, B. Chiaro, A. Dunsworth, A. Fowler, E. Jeffrey, J. Kelly, E. Lucero, J. Mutus, P. J. J. O'Malley, M. Neeley, C. Quintana, D. Sank, A. Vainsencher, J. Wenner, T. White, E. Kapit, H. Neven, and J. Martinis, "Chiral ground-state currents of interacting photons in a synthetic magnetic field," Nat. Phys. **13**, 146–151 (2017).

[122] P. Roushan, C. Neill, J. Tangpanitanon, V. M. Bastidas, A. Megrant, R. Barends, Y. Chen, Z. Chen, B. Chiaro, A. Dunsworth, A. Fowler, B. Foxen, M. Giustina, E. Jeffrey, J. Kelly, E. Lucero, J. Mutus, M. Neeley, C. Quintana, D. Sank, A. Vainsencher, J. Wenner, T. White, H. Neven, D. G. Angelakis, and J. Martinis, "Spectroscopic signatures of localization with interacting photons in superconducting qubits," Science **358**, 1175–1179 (2017).

[123] A. J. Kollár, M. Fitzpatrick, and A. A. Houck, "Hyperbolic lattices in circuit quantum electrodynamics," Nature **571**, 45–50 (2019).

[124] V. V. Albert, L. I. Glazman, and L. Jiang, "Topological properties of linear circuit lattices," Phys. Rev. Lett. **114**, 173902 (2015).

[125] E. I. Rosenthal, N. K. Ehrlich, M. S. Rudner, A. P. Higginbotham, and K. W. Lehnert, "Topological phase transition measured in a dissipative metamaterial," Phys. Rev. B **97**, 220301 (2018).

[126] C. H. Lee, S. Imhof, C. Berger, F. Bayer, J. Brehm, L. W. Molenkamp, T. Kiessling, and R. Thomale, "Topolectrical circuits," Commun. Phys. **1**, 39 (2018).

[127] S. Imhof, C. Berger, F. Bayer, J. Brehm, L. W. Molenkamp, T. Kiessling, F. Schindler, C. H. Lee, M. Greiter, T. Neupert, and R. Thomale, "Topolectrical-circuit realization of topological corner modes," Nat. Phys. **14**, 925–929 (2018).

[128] S. Liu, W. Gao, Q. Zhang, S. Ma, L. Zhang, C. Liu, Y. J. Xiang, T. J. Cui, and S. Zhang, "Topologically protected edge state in two-dimensional Su–Schrieffer–Heeger circuit," Research **2019**, 8609875.

[129] M. Serra-Garcia, R. Süsstrunk, and S. D. Huber, "Observation of quadrupole transitions and edge mode topology in an LC circuit network," Phys. Rev. B **99**, 020304 (2019).

[130] F. Zangeneh-Nejad and R. Fleury, "Nonlinear second-order topological insulators," Phys. Rev. Lett. **123**, 053902 (2019).

[131] T. Kotwal, H. Ronellenfitsch, F. Moseley, A. Stegmaier, R. Thomale, and J. Dunkel, "Active topolectrical circuits," arXiv:1903.10130 (2019).

[132] R. Süsstrunk and S. D. Huber, "Observation of phononic helical edge states in a mechanical topological insulator," Science **349**, 47–50 (2015).

[133] D. D. Snee and Y.-P. Ma, "Edge solitons in a nonlinear mechanical topological insulator," Extreme Mech. Lett. **30**, 100487 (2019).

[134] R. Chaunsali and G. Theocharis, "Self-induced topological transition in phononic crystals by nonlinearity management," Phys. Rev. B **100**, 014302 (2019).

[135] Y. Lumer, M. C. Rechtsman, Y. Plotnik, and M. Segev, "Instability of bosonic topological edge states in the presence of interactions," Phys. Rev. A **94**, 021801 (2016).

[136] D. Solnyshkov, O. Bleu, B. Teklu, and G. Malpuech, "Chirality of topological gap solitons in bosonic dimer chains," Phys. Rev. Lett. **118**, 023901 (2017).

[137] D. A. Smirnova, L. A. Smirnov, D. Leykam, and Y. S. Kivshar, "Topological edge states and gap solitons in the nonlinear Dirac model," Laser Photonics Rev. **13**, 1900223 (2019).

[138] W. Zhang, X. Chen, Y. V. Kartashov, V. V. Konotop, and F. Ye, "Coupling of edge states and topological Bragg solitons," Phys. Rev. Lett. **123**, 254103 (2019).

[139] D. Leykam and Y. D. Chong, "Edge solitons in nonlinear-photonic topological insulators," Phys. Rev. Lett. **117**, 143901 (2016).

[140] A. N. Poddubny and D. A. Smirnova, "Ring Dirac solitons in nonlinear topological systems," Phys. Rev. A **98**, 013827 (2018).

[141] J. Liu and L. B. Fu, "Berry phase in nonlinear systems," Phys. Rev. A **81**, 052112 (2010).

[142] R. W. Bomantara, W. Zhao, L. Zhou, and J. Gong, "Nonlinear Dirac cones," Phys. Rev. B **96**, 121406 (2017).

[143] D. D. Solnyshkov, O. Bleu, and G. Malpuech, "Topological optical isolator based on polariton graphene," Appl. Phys. Lett. **112**, 031106 (2018).

[144] Y. Hadad, A. B. Khanikaev, and A. Alù, "Self-induced topological transitions and edge states supported by nonlinear staggered potentials," Phys. Rev. B **93**, 155112 (2016).

[145] Y. Lumer, Y. Plotnik, M. C. Rechtsman, and M. Segev, "Self-localized states in photonic topological insulators," Phys. Rev. Lett. **111**, 243905 (2013).

[146] D. R. Gulevich, D. Yudin, D. V. Skryabin, I. V. Iorsh, and I. A. Shelykh, "Exploring nonlinear topological states of matter with exciton-polaritons: Edge solitons in Kagome lattice," Sci. Rep. **7**, 1780 (2017).

[147] J. L. Marzuola, M. Rechtsman, B. Osting, and M. Bandres, "Bulk soliton dynamics in bosonic topological insulators," arXiv:1904.10312 (2019).

[148] S. Mukherjee and M. C. Rechtsman, "Observation of Floquet solitons in a topological bandgap," Science **368**, 856 (2020).).

[149] M. J. Ablowitz, C. W. Curtis, and Y.-P. Ma, "Linear and nonlinear traveling edge waves in optical honeycomb lattices," Phys. Rev. A **90**, 023813 (2014).

[150] Y. V. Kartashov and D. V. Skryabin, "Modulational instability and solitary waves in polariton topological insulators," Optica **3**, 1228 (2016).

[151] J. Cuevas-Maraver, P. G. Kevrekidis, A. Saxena, A. Comech, and R. Lan, "Stability of solitary waves and vortices in a 2D nonlinear Dirac model," Phys. Rev. Lett. **116**, 214101 (2016).

[152] J. Cuevas-Maraver, P. G. Kevrekidis, A. B. Aceves, and A. Saxena, "Solitary waves in a two-dimensional nonlinear Dirac equation: From discrete to continuum," J. Phys. A **50**, 495207 (2017).

[153] J. Cuevas-Maraver, N. Boussaïd, A. Comech, R. Lan, P. G. Kevrekidis, and A. Saxena, "Solitary waves in the nonlinear Dirac equation," in *Understanding Complex Systems* (Springer International Publishing, 2018), pp. 89–143.

[154] Y. Hadad, V. Vitelli, and A. Alu, "Solitons and propagating domain walls in topological resonator arrays," ACS Photonics **4**, 1974–1979 (2017).

[155] O. Bleu, D. D. Solnyshkov, and G. Malpuech, "Interacting quantum fluid in a polariton Chern insulator," Phys. Rev. B **93**, 085438 (2016).

[156] C. Li, F. Ye, X. Chen, Y. V. Kartashov, A. Ferrando, L. Torner, and D. V. Skryabin, "Lieb polariton topological insulators," Phys. Rev. B **97**, 081103 (2018).

[157] M. Ezawa, "Higher-order topological insulators and semimetals on the breathing Kagome and pyrochlore lattices," Phys. Rev. Lett. **120**, 026801 (2018).

[158] M. I. Shalaev, S. Desnavi, W. Walasik, and N. M. Litchinitser, "Reconfigurable topological photonic crystal," New J. Phys. **20**, 023040 (2018).

[159] O. Bleu, G. Malpuech, and D. D. Solnyshkov, "Robust quantum valley Hall effect for vortices in an interacting bosonic quantum fluid," Nat. Commun. **9**, 3991 (2018).

[160] P. St-Jean, V. Goblot, E. Galopin, A. Lemaître, T. Ozawa, L. L. Gratiet, I. Sagnes, J. Bloch, and A. Amo, "Lasing in topological edge states of a one-dimensional lattice," Nat. Photonics **11**, 651 (2017).

[161]M. Parto, S. Wittek, H. Hodaei, G. Harari, M. A. Bandres, J. Ren, M. C. Rechtsman, M. Segev, D. N. Christodoulides, and M. Khajavikhan, "Edge-mode lasing in 1D topological active arrays," Phys. Rev. Lett. **120**, 113901 (2018).

[162]H. Zhao, P. Miao, M. H. Teimourpour, S. Malzard, R. El-Ganainy, H. Schomerus, and L. Feng, "Topological hybrid silicon microlasers," Nat. Commun. **9**, 981 (2018).

[163]C. Han, M. Lee, S. Callard, C. Seassal, and H. Jeon, "Lasing at topological edge states in a photonic crystal L3 nanocavity dimer array," Light: Sci. Appl. **8**, 40 (2019).

[164]S. Klembt, T. H. Harder, O. A. Egorov, K. Winkler, R. Ge, M. A. Bandres, M. Emmerling, L. Worschech, T. C. H. Liew, M. Segev, C. Schneider, and S. Höfling, "Exciton-polariton topological insulator," Nature **562**, 552 (2018).

[165]J. Ohtsubo, *Semiconductor Lasers: Stability, Instability, and Chaos* (Springer, 2007).

[166]S. Longhi, Y. Kominis, and V. Kovanis, "Presence of temporal dynamical instabilities in topological insulator lasers," Europhys. Lett. **122**, 14004 (2018).

[167]S. Longhi and L. Feng, "Invited article: Mitigation of dynamical instabilities in laser arrays via non-Hermitian coupling," APL Photonics **3**, 060802 (2018).

[168]H. Schomerus, "Topologically protected midgap states in complex photonic lattices," Opt. Lett. **38**, 1912 (2013).

[169]S. Weimann, M. Kremer, Y. Plotnik, Y. Lumer, S. Nolte, K. G. Makris, M. Segev, M. C. Rechtsman, and A. Szameit, "Topologically protected bound states in photonic parity-time-symmetric crystals," Nat. Mater. **16**, 433 (2017).

[170]S. Malzard and H. Schomerus, "Nonlinear mode competition and symmetry-protected power oscillations in topological lasers," New J. Phys. **20**, 063044 (2018).

[171]S. Malzard, E. Cancellieri, and H. Schomerus, "Topological dynamics and excitations in lasers and condensates with saturable gain or loss," Opt. Express **26**, 22506–22518 (2018).

[172]E. Cancellieri and H. Schomerus, "$\mathcal{PC}$-symmetry-protected edge states in interacting driven-dissipative bosonic systems," Phys. Rev. A **99**, 033801 (2019).

[173]S. Longhi, "Non-Hermitian gauged topological laser arrays," Ann. Phys. **530**, 1800023 (2018).

[174]Z. Gong, Y. Ashida, K. Kawabata, K. Takasan, S. Higashikawa, and M. Ueda, "Topological phases of non-Hermitian systems," Phys. Rev. X **8**, 031079 (2018).

[175]S. Longhi, "Non-Hermitian topological phase transition in PT-symmetric mode-locked lasers," Opt. Lett. **44**, 1190–1193 (2019).

[176]M. Secli and I. Carusotto, "Harper-Hofstadter topological laser with frequency-dependent gain," in *2019 Conference on Lasers and Electro-Optics Europe & European Quantum Electronics Conference (CLEO/Europe-EQEC)* (IEEE, 2019).

[177]B. Bahari, L.-Y. Hsu, S. H. Pan, D. Preece, A. Ndao, A. E. Amili, Y. Fainman, and B. Kanté, "Topological lasers generating and multiplexing topological light," arXiv:1904.11873 (2019).

[178]G. Harari, M. A. Bandres, Y. Lumer, M. C. Rechtsman, Y. D. Chong, M. Khajavikhan, D. N. Christodoulides, and M. Segev, "Topological insulator laser: Theory," Science **359**, eaar4003 (2018).

[179]Y. V. Kartashov and D. V. Skryabin, "Two-dimensional topological polariton laser," Phys. Rev. Lett. **122**, 083902 (2019).

[180]F. Baboux, D. D. Bernardis, V. Goblot, V. N. Gladilin, C. Gomez, E. Galopin, L. L. Gratiet, A. Lemaître, I. Sagnes, I. Carusotto, M. Wouters, A. Amo, and J. Bloch, "Unstable and stable regimes of polariton condensation," Optica **5**, 1163 (2018).

[181]M. Seclì, M. Capone, and I. Carusotto, "Theory of chiral edge state lasing in a two-dimensional topological system," Phys. Rev. Res. **1**, 033148 (2019).

[182]I. Amelio and I. Carusotto, "Theory of the coherence of topological lasers," arXiv:1911.10437 (2019).

[183]A. Loirette-Pelous, "Dynamical stability of 2d topological lasers," arXiv:1912.03911 (2019).

[184]S. K. Ivanov, Y. Zhang, Y. V. Kartashov, and D. V. Skryabin, "Floquet topological insulator laser," APL Photonics **4**, 126101 (2019).

[185]S. Pourjamal, T. K. Hakala, M. Nečada, F. Freire-Fernández, M. Kataja, H. Rekola, J.-P. Martikainen, P. Törmä, and S. van Dijken, "Lasing in Ni nanodisk arrays," ACS Nano **13**, 5686–5692 (2019).

[186]X.-C. Sun and X. Hu, "Topological ring-cavity laser formed by honeycomb photonic crystals," arXiv:1906.02464 (2019).

[187]H. Zhong, Y. Li, D. Song, Y. V. Kartashov, Y. Zhang, Y. Zhang, and Z. Chen, "Topological valley Hall edge state lasing," arXiv:1912.13003 (2019).

[188]Y. Gong, S. Wong, A. J. Bennett, D. L. Huffaker, and S. S. Oh, "Topological insulator laser using valley-Hall photonic crystals," arXiv:2001.03661 (2020).

[189]Z.-K. Shao, H.-Z. Chen, S. Wang, X.-R. Mao, Z.-Q. Yang, S.-L. Wang, X.-X. Wang, X. Hu, and R.-M. Ma, "A high-performance topological bulk laser based on band-inversion-induced reflection," Nat. Nanotechnol. **15**, 67 (2020).

[190]X. Gao, L. Yang, H. Lin, L. Zhang, J. Li, F. Bo, Z. Wang, and L. Lu, "Dirac-vortex topological cavity," arXiv:1911.09540 (2019).

[191]L. Pilozzi and C. Conti, "Topological cascade laser for frequency comb generation in PT-symmetric structures," Opt. Lett. **42**, 5174–5177 (2017).

[192]Z. Yang, E. Lustig, G. Harari, Y. Plotnik, Y. Lumer, M. A. Bandres, and M. Segev, "Mode-locked topological insulator laser utilizing synthetic dimensions," Phys. Rev. X **10**, 011059 (2020).

[193]H. Suchomel, S. Klembt, T. H. Harder, M. Klaas, O. A. Egorov, K. Winkler, M. Emmerling, R. Thomale, S. Höfling, and C. Schneider, "Platform for electrically pumped polariton simulators and topological lasers," Phys. Rev. Lett. **121**, 257402 (2018).

[194]Y. Zeng, U. Chattopadhyay, B. Zhu, B. Qiang, J. Li, Y. Jin, L. Li, A. G. Davies, E. H. Linfield, B. Zhang, Y. Chong, and Q. J. Wang, "Electrically pumped topological laser with valley edge modes," Nature **578**, 246–250 (2020).

[195]S. Kruk, A. Slobozhanyuk, D. Denkova, A. Poddubny, I. Kravchenko, A. Miroshnichenko, D. Neshev, and Y. Kivshar, "Edge states and topological phase transitions in chains of dielectric nanoparticles," Small **13**, 1603190 (2017).

[196]R. Landauer, "Parametric amplification along nonlinear transmission lines," J. Appl. Phys. **31**, 479–484 (1960).

[197]C.-E. Bardyn, T. Karzig, G. Refael, and T. C. H. Liew, "Chiral Bogoliubov excitations in nonlinear bosonic systems," Phys. Rev. B **93**, 020502 (2016).

[198]H. Sigurdsson, G. Li, and T. C. H. Liew, "Spontaneous and superfluid chiral edge states in exciton-polariton condensates," Phys. Rev. B **96**, 115453 (2017).

[199]V. Peano, M. Houde, C. Brendel, F. Marquardt, and A. A. Clerk, "Topological phase transitions and chiral inelastic transport induced by the squeezing of light," Nat. Commun. **7**, 10779 (2016).

[200]V. Peano, M. Houde, F. Marquardt, and A. A. Clerk, "Topological quantum fluctuations and traveling wave amplifiers," Phys. Rev. X **6**, 041026 (2016).

[201]J. W. You, Z. Lan, and N. C. Panoiu, "Four-wave mixing of topological edge plasmons in graphene metasurfaces," Science Adv. **6**, eaaz3910 (2020).

[202]A. Blanco-Redondo, B. Bell, D. Oren, B. J. Eggleton, and M. Segev, "Topological protection of biphoton states," Science **362**, 568–571 (2018).

[203]M. Wang, C. Doyle, B. Bell, M. J. Collins, E. Magi, B. J. Eggleton, M. Segev, and A. Blanco-Redondo, "Topologically protected entangled photonic states," Nanophotonics **8**, 1327–1335 (2019).

[204]A. Blanco-Redondo, I. Andonegui, M. J. Collins, G. Harari, Y. Lumer, M. C. Rechtsman, B. J. Eggleton, and M. Segev, "Topological optical waveguiding in silicon and the transition between topological and trivial defect states," Phys. Rev. Lett. **116**, 163901 (2016).

[205]I. Martin, G. Refael, and B. Halperin, "Topological frequency conversion in strongly driven quantum systems," Phys. Rev. X **7**, 041008 (2017).

[206]E. Lustig, S. Weimann, Y. Plotnik, Y. Lumer, M. A. Bandres, A. Szameit, and M. Segev, "Photonic topological insulator in synthetic dimensions," Nature **567**, 356–360 (2019).

[207]A. Dutt, M. Minkov, Q. Lin, L. Yuan, D. A. B. Miller, and S. Fan, "Experimental band structure spectroscopy along a synthetic dimension," Nat. Commun. **10**, 3122 (2019).

[208]A. Dutt, Q. Lin, L. Yuan, M. Minkov, M. Xiao, and S. Fan, "A single photonic cavity with two independent physical synthetic dimensions," Science **367**, 59–64 (2020).

[209]B. A. Bell, K. Wang, A. S. Solntsev, D. N. Neshev, A. A. Sukhorukov, and B. J. Eggleton, "Spectral photonic lattices with complex long-range coupling," Optica **4**, 1433–1436 (2017).

[210]I. Carusotto and C. Ciuti, "Quantum fluids of light," Rev. Mod. Phys. **85**, 299–366 (2013).

[211]C. Noh and D. G. Angelakis, "Quantum simulations and many-body physics with light," Rep. Prog. Phys. **80**, 016401 (2017).

[212]M. Di Liberto, A. Recati, I. Carusotto, and C. Menotti, "Two-body physics in the Su-Schrieffer-Heeger model," Phys. Rev. A **94**, 062704 (2016).

[213]M. A. Gorlach and A. N. Poddubny, "Topological edge states of bound photon pairs," Phys. Rev. A **95**, 053866 (2017).

[214]M. A. Gorlach, M. Di Liberto, A. Recati, I. Carusotto, A. N. Poddubny, and C. Menotti, "Simulation of two-boson bound states using arrays of driven-dissipative coupled linear optical resonators," Phys. Rev. A **98**, 063625 (2018).

[215]N. A. Olekhno, E. I. Kretov, A. A. Stepanenko, P. A. Ivanova, V. V. Yaroshenko, E. M. Puhtina, D. S. Filonov, B. Cappello, L. Matekovits, and M. A. Gorlach, "Topological edge states of interacting photon pairs realized in a topolectrical circuit," Nat. Commun. **11**, 1436 (2020).

[216]G. Salerno, G. Palumbo, N. Goldman, and M. D. Liberto, "Interaction-induced lattices for bound states: Designing flat bands, quantized pumps, and higher-order topological insulators for doublons," Phys. Rev. Res. **2**, 013348 (2020).

[217]D. Rossini and R. Fazio, "Mott-insulating and glassy phases of polaritons in 1D arrays of coupled cavities," Phys. Rev. Lett. **99**, 186401 (2007).

[218]I. Carusotto, D. Gerace, H. E. Tureci, S. De Liberato, C. Ciuti, and A. Imamoğlu, "Fermionized photons in an array of driven dissipative nonlinear cavities," Phys. Rev. Lett. **103**, 033601 (2009).

[219]J. Tangpanitanon, S. R. Clark, V. M. Bastidas, R. Fazio, D. Jaksch, and D. G. Angelakis, "Hidden order in quantum many-body dynamics of driven-dissipative nonlinear photonic lattices," Phys. Rev. A **99**, 043808 (2019).

[220]H. Alaeian, C. W. S. Chang, M. V. Moghaddam, C. M. Wilson, E. Solano, and E. Rico, "Creating lattice gauge potentials in circuit QED: The bosonic Creutz ladder," Phys. Rev. A **99**, 053834 (2019).

[221]R. Rota and V. Savona, "Simulating frustrated antiferromagnets with quadratically driven QED cavities," Phys. Rev. A **100**, 013838 (2019).

[222]W. Nie, Z. H. Peng, F. Nori, and Y.-X. Liu, "Topologically protected quantum coherence in a superatom," Phys. Rev. Lett. **124**, 023603 (2020).

[223]J. Tangpanitanon, V. M. Bastidas, S. Al-Assam, P. Roushan, D. Jaksch, and D. G. Angelakis, "Topological pumping of photons in nonlinear resonator arrays," Phys. Rev. Lett. **117**, 213603 (2016).

[224]T. Haug, L. Amico, L.-C. Kwek, W. J. Munro, and V. M. Bastidas, "Topological pumping of quantum correlations," Phys. Rev. Res. **2**, 013135 (2020).

[225]J. Cho, D. G. Angelakis, and S. Bose, "Fractional quantum Hall state in coupled cavities," Phys. Rev. Lett. **101**, 246809 (2008).

[226]R. O. Umucalilar and I. Carusotto, "Fractional quantum Hall states of photons in an array of dissipative coupled cavities," Phys. Rev. Lett. **108**, 206809 (2012).

[227]M. Hafezi, M. D. Lukin, and J. M. Taylor, "Non-equilibrium fractional quantum Hall state of light," New J. Phys. **15**, 063001 (2013).

[228]D. A. Smirnova, P. Padmanabhan, and D. Leykam, "Parity anomaly laser," Opt. Lett. **44**, 1120–1123 (2019).

[229]M. I. Shalaev, W. Walasik, and N. M. Litchinitser, "Optically tunable topological photonic crystal," Optica **6**, 839 (2019).

[230]Z. A. Kudyshev, A. V. Kildishev, A. Boltasseva, and V. M. Shalaev, "Photonic topological phase transition on demand," Nanophotonics **8**, 1349–1356 (2019).

[231]Z. A. Kudyshev, A. V. Kildishev, A. Boltasseva, and V. M. Shalaev, "Tuning topology of photonic systems with transparent conducting oxides," ACS Photonics **6**, 1922–1930 (2019).